The Effect of the Boundary Layer present in Wind Tunnels on the Aerodynamic Drag of a Model Truck

Thomas Lutz

September 1997

Submitted in Partial Fulfillment for an MSc. Degree

SYNOPSIS

This thesis deals with a system that reduces the oncoming boundary layer displacement thickness in a wind tunnel. The device is then used to examine the effect that this boundary layer has on the aerodynamic drag of a standard truck, which is classified as a bluff body with a high ground clearance and the same truck fitted with skirts all round, which is then classified as a bluff body with a low ground clearance.

To gain insight into this field of industrial aerodynamics, an extensive literature survey was done in which all the relevant SAE papers onwards from the late sixties were studied and summarised in the first section of this report.

The second section deals with a system that can limit the boundary layer displacement thickness in the test section of the 3/4 open jet wind tunnel. Through investigations and an extensive literature research a suction device was designed and built. This boundary layer removal system was then tested to ensure that the main flow indicators are not influenced by the suction and thus lie within internationally accepted limits. Included in this section are a description of the truck model and the other instruments or devices used to complete the testing.

The third section deals with the aerodynamic drag experienced by the bluff body with a high ground clearance.

Included in the third section is an investigation that deals with the aerodynamic drag of the same truck model, when skirting has been added which considerably lowers the ground clearance.

The results obtained from the above investigations indicate that the drag of the

model without skirts is increased by about 3.8% with the removal of the boundary layer and up to 10% for the model with the skirts. It is thus shown that the farther the object protrudes into the boundary layer, the larger the increase in drag will be once this boundary layer has been removed. These figures were obtained from testing the model at 22.2m/s free stream velocity and a 6mm wheel-ground clearance, with the wheels rotating.

TABLE OF CONTENTS

LIST OF ILLUSTRATIONS

NOMENCLATURE

Symbol	*Description*	*Units*
v	Velocity	m/s
u	Velocity	m/s
P	Pressure	Pa
ΔP	Pressure difference	Pa
ρ	Density	kg/m^3
v_a	Actual Velocity	m/s
v_m	Measured Velocity	m/s
v_s	Free Stream Velocity	m/s
u_∞	Free Stream Velocity	m/s
t	Time	s
δ	BL Thickness	m
δ^*	BL Displ. Thickness	m
F	Force	N
C_D	Drag Coefficient	no units
ψ	Yaw Angle	degrees

ACKNOWLEDGEMENTS

I would like to thank Professor Tony Sayers for his valuable time and contribution towards the completion of this thesis. His guidance through some of the more complex stages of this work was extremely useful and intuitive.

My thanks also go to every member of the workshop team. The technicians and their helpers were always there when needed and always had time to help when parts needed machining or advice was required.

Finally my thanks go to the rest of the staff of the Mechanical Engineering Department who made the duration of the research a very enjoyable experience.

CHAPTER 1 - INTRODUCTION

Many prototypes in our current day and age are most often preceded by some kind of scale model. The most important reasons for building scale models is that they are cheaper than the prototype due to smaller sizes and less man - hours involved. If the scale model is a true and correct reflection of the prototype incorporating all the details, the behaviour of the prototype can be predicted by analysing the performance of the scale model. Further, if changes need to be made, only a new scale model will have to be built, compared to building a new prototype. This is of special importance to the automotive and aeronautical industries where a prototype can require thousands of man – hours and millions of Dollars to build. Keeping the costs as low as possible during the design and development stages will help to keep the company competitive in terms of design costs and can certainly influence the later sales through keeping the price of the product lower than a comparable product from rival companies.

An analysis of the aerodynamic behaviour of bluff bodies in ground proximity can best be accomplished by inserting the body into a wind tunnel. One of the most important requirements of scale model testing is that the results obtained therefrom reflect an accurate picture of the prototype's behaviour. If this cannot be guaranteed, then the results obtained will not accurately reflect the prototype performance and the entire testing was in vain. It is thus of fundamental importance that the scale model testing reflect actual prototype behaviour to the highest degree possible. This means that the testing procedure may not introduce factors that are not experienced by the later version in day to day operations.

Classical wind tunnel testing is characterised by a model resting on a balance and the air is blown against the model. The model then experiences an array of forces

and these forces are then measured by the wind tunnel balance.

This procedure however introduces a factor, which is not experienced in day to day operation of ground vehicles. When the air is blown across the wind tunnel floor and its walls, a boundary layer forms. The boundary layer arises due to the relative velocity between the air and the floor of the wind tunnel. This boundary layer is most importantly characterised by a lower average velocity than the free stream velocity. In normal operations the prototype would drive over a road into still air, and be confronted with a vertical velocity profile, assuming no wind is blowing and thus experiencing no relative velocity between ground and air. In the wind tunnel the model experiences a parabolic velocity profile in the boundary layer and only a vertical profile in the free stream. This effectively means that in the wind tunnel, the mass flow rate of air is lower due to the lower average velocity in the boundary layer and thus the experienced aerodynamic drag will be less than it should be.

Factors like the amount of ground clearance between model and floor and the underfloor detail of the model can also not be investigated properly anymore, because these regions lie within the boundary layer flow of the wind tunnel. This boundary flow does not only affect drag, but also lift. This is a problem that many racing car designers are faced with.

The objective of this report is to investigate the effect that the boundary layer flow has on the aerodynamic drag of two bluff bodies, one being a truck which has a high ground clearance and the other being the same truck with a lower ground clearance.

The wind tunnel boundary layer will be removed with the aid of boundary suction. This is a device that effectively introduces energy into the overall flow by removing, i.e sucking away, the retarded boundary layer flow. This will result in the model

experiencing a near vertical velocity profile and thus a higher mass flow striking it.

This suction device is designed and built. It is then subject to a variety of tests to ensure that the flow quality is not jeopardised by the introduction of the suction system. Once the testing is complete and a flow of high quality assured, the testing of the models will commence.

Both models have rotating wheels, as it was found in the literature research that rotating wheels cause pressure fields about the model, especially close to the ground, which affect the flow in ground proximity. The models will be tested with wheels rotating and not rotating, suction on and off and at various ground clearances.

CHAPTER 2 - LITERATURE SURVEY

This Chapter will list and compare the most important aspects from 21 SAE papers that deal with this topic. Accordingly, this Chapter will analyse the information under the following headings.

- Model Descriptions
- Test Conditions
- Experimental Method 1: Boundary Layer Removal through Moving Ground
- Experimental Method 2: Boundary Layer Removal through Suction
- Experimental Method 3: Boundary Layer Removal by employing a Ground Board
- Results

In turn, each of these heading is sub – divided to specifically deal with various topics.

MODEL DESCRIPTIONS

"The most important influence on aerodynamic drag is the longitudinal cab-container gap, the model ground clearance and the relative geometries of each"[1].

Model Size

Most authors of the reviewed literature felt that the models should range in size from a 1:7 scale to not smaller than a 1:10 scale to yield accurate data. One author felt

that tests should not be conducted at sizes less than 1:3 [16], because compressibility effects due to the required high Reynolds Number for dynamic similarity might corrupt data. For the same type of investigation, another researcher opted for a 1:12 scale model, and achieved satisfactory results with it [19].

Model Detail

All researchers were in agreement that a very high degree of model detail was essential in determining the correct aerodynamic characteristics of models. Simply reproducing the rough geometry of the model was not considered as adequate. This includes underfloor model detail as well as lamps, mirrors, horns etc.

Model Simulation

Some research indicated that an analysis of the boundary layer on aerodynamic drag must include an examination of the influence of wheel rotation on the overall drag. This was an important factor when considering the influence due to the close proximity of the wheels to the boundary layer[17]. One author felt that modeling the static tyre deflection would be enough[15].

TEST CONDITIONS

Examining the model in the correct environment is a prerequisite for realistic results. Apart from the published SAE Recommendations J1252, the literature survey revealed the following points and discrepancies.

Reynolds Number

Probably the biggest disagreement in this survey was identified with the range of allowable Reynolds Numbers. SAE J1252[22] recommends a minimum Reynolds Number of 700000. [2] recommends numbers from 2200000 to 4400000, but conceded that this range did not influence the drag coefficient and ultimately settled for a Reynolds Number of 1700000. The other papers featured tests conducted from 300000 [3] to 4400000, with the drag coefficient only varying slightly. [15] found that the drag coefficient decreased from a Reynolds number of 780000 to 1500000. Some authors felt that the turbulence intensity experienced in the wind tunnels influenced the Reynolds Number, resulting in a higher Reynolds Number for wind tunnels with higher turbulence intensities[3].

Reynolds numbers are based on a parameter of the model. This parameter could be the square root of the frontal area [6], the width of the model [4] or the length of the model [19].

Boundary Layer Thickness and Ground Clearance.

All research indicated that in order to achieve realistic results, the boundary layer approaching the model at the front axle must be kept to an absolute minimum. The boundary layer should further be kept as small as possible compared to the ground

height to prevent boundary layer separation due to the superposed pressure field of the model [11]. If the boundary layer thickness was less than 10% of the ground clearance, then the effect of the boundary layer on the aerodynamic drag would be negligible [14]. For the moving ground, [12] felt that the wheels should be kept in contact with the ground and allowed to rotate. [18] felt that that the ground clearance be restricted to 5% of the vehicle height. The combined influence of wheel rotation and ground clearance on the drag might be larger than the influence of the boundary layer itself [6].

Air Stream Quality

Some authors, especially [10], felt that a detailed survey of the air stream entering the test section should be undertaken once the boundary layer removal system is in place. SAE J1252[22] must be consulted and [11] further advised on the parameters that must be investigated, the most important one being the axial static pressure coefficient and the dynamic pressure distribution.

EXPERIMENTAL METHOD 1: BOUNDARY LAYER REMOVAL THROUGH MOVING GROUND

Model Support

All authors agree that the model must be mounted securely on or above the belt. No deflection due to aerodynamic forces can be allowed. The model is either mounted

from above [18] or from behind via a rear sting [6], with an internal balance that measures the forces.

For the case where the model rests on the belt, a friction calibration will be necessary to determine the rolling friction [9].

Moving Ground

The belt should be able to run at the same speed as the air is blowing. This will allow synchronous testing. Varying the speed of the belt will change the thickness of the boundary layer [18], as reducing the moving ground speed has a similar effect on the base pressure to a reduction in model ground clearance. At a speed of 30m/s, a local velocity distribution of within 2 to 5% within the free stream velocity can be achieved [17].

The entire assembly, belt and model, must be yawed to simulate correct cross-wind conditions [12].

The oncoming boundary layer must be removed, either by suction [17], or a boundary layer scoop [6]. The removed air must be re-introduced into the wind tunnel for closed test sections aft of the test section.

Flaps at the trailing edge of the belt can change the circulation, changing the setting of these flaps can set the stagnation streamline exactly onto the nose of the cover plate [6]. Further, it was found that flow separation at the leading edge of the moving belt due to the superposed pressure field of the model caused a thickening of the boundary layer.

The idea of the moving ground is to draw more air under the model [12]. The ideal test condition is the one where the mass flux under the model equals the mass flux under the truck on the open road [6].

Experimental Methods: Boundary Layer Removal through Suction

A suction system can clearly show the influence of the boundary layer on the aerodynamic drag. The suction system uses a perforated surface through which the boundary layer is sucked off. A detailed description of an existing suction system is found in [22], which describes the suction system used in the Porsche Wind Tunnel. However, this system needs a larger area in front of the model because the suction system tends to be sensitive to the superposed pressure field of the model [6].
The boundary layer is to be kept as thin as possible. The remaining problem is then that the lower mass flux below the model must be accounted for.
The advantage of the suction system over the moving belt is that separation of the boundary layer due to the superposed pressure field by the model is avoided [17], thereby doing away with the flaps that are required to tune the stagnation point to the leading edge of the belt.

Experimental Methods: Boundary Layer Control through a Ground Board

The ground board can be used to deliver only a very thin boundary layer. It is cheaper and easier to construct than a moving ground or a suction system [4].
The boundary layer will only form over the ground board and thus be considerably thinner than on the wind tunnel floor.
The ground board is impermeable, and extends completely across the test section. Furthermore, it must extend more than two body-widths upstream and more than 6 body-widths downstream of the model.
However, flaps are again required to tune the stagnation streamline to the leading edge [10].

The model over a fixed ground plane should be raised by the boundary layer displacement thickness [10].

RESULTS

All ground simulation effectively reduces the boundary layer thickness. [18] achieved a reduction of 58% and for the boundary layer displacement thickness a reduction of 90%. [6] achieved a reduction from 155mm to 20mm of the boundary layer with the scoop and the moving ground. A reduction from 24mm to 9mm was achieved by [9] for the same arrangement. Similar results were achieved in the Porsche Wind Tunnel[22].

Aerodynamic drag is seen to increase with no ground simulation [9]. Floor movement increases the drag by between 5 to 8% [17]. Boundary layer suction yielded increased drag results of between 1.3 to 3.7% for a natural boundary layer height of 85mm [14].

The drag coefficient remained fairly constant for belt speeds of 50% of the wind speed upwards [6].

Some authors [3] felt that a difference in drag coefficients between on-road and wind tunnel testing stem from lower turbulence intensities in the wind tunnels, which in turn affect the Reynolds Number. Tests at low turbulence intensities over-predict the aerodynamic drag. The same author further found that as long as the boundary layer thickness was clearly less than the ground clearance, no significant errors would be introduced.

CHAPTER 3 - EXPERIMENTAL APPARATUS

Through an extensive literature research the only effective means by which the boundary layer can be removed and prevented from forming is either by employing a moving ground or using suction to remove the slower moving layers of air close to the ground.

Both systems provide energy to the ground layer. The belt accelerates the slower moving layers of the boundary flow to the speed of the free stream air, assuming that the belt runs at the same speed as the air, and thus feeds energy into these slower moving layers. The suction system does this by removing the retarded flow of the boundary layer from the test section and accordingly high energy fluid is transported to the near wall region from the main stream.

The moving ground is the better of the two options and would require a conveyor belt that could run at the same speed as the air that is blown against the stationary object. This means that the belt would have to run at a speed of up to 120km/h.

Preliminary investigations and designs for such a system showed that such a system would be very difficult to set up and would be very expensive. Due to the high speed of the belt, large accelerations will be experienced by the belt over the idling, tightening and driving pulleys. Accordingly, the belt would tend to wander off to one side and render the system unstable. To introduce some degree of stability into the system, the idling pulley should effectively be used as a straightener pulley. This means that the pulley should be able to slide by means of pneumatic cylinders. As soon as the belt sensor would sense that the belt is running onto to one side, the cylinder on that side would be driven out and force the pulley outwards. This action will result in the belt moving towards the centre again. This is essentially a closed

loop feedback system and requires the use of complicated pneumatic equipment and PLC's. Due to the high speed of the system, one of the belt tightners pulleys would also require this feature.

Tapered rollers, rubberised to minimise axial motion of the belt, high speed bearings and a very complex belt structure were further required. A motor and gearbox would also be necessary. In order to match the belt speed to the air speed, the motor would be fitted with a variable speed drive that would allow the operator to set the motor speed at the required rpm. For calculation purposes a rotary encoder with a digital read out of the motor speed would also become necessary.

The above belt assembly would have to be mounted on a platform that could be yawed to allow for the determination of the drag coefficient at various wind directions. This would add a further complexity to the design.

Due to the moving ground running below the model, the balance would have to be mounted above the model. The balance is used to measure the drag force experienced by the model at a specific yaw angle and wind speed. This would require a slight modification to the existing balance.

Taking the above complexities into consideration and the time span and finally also the capital outlay, it was decided to abandon this method of removing and suppressing the boundary layer. It was decided to focus the attention on the easier and by far cheaper way of using ground suction to remove and suppress the boundary layer.

Initial designs and cost estimates for the moving ground are in Appendix A.

REMOVAL OF THE BOUNDARY THROUGH MOVING GROUND

DESIGN CRITERIA

The apparatus that will simulate the moving ground must fulfil the following requirements

- It must be mobile so that it can be moved out of the test section to allow other students access to the test section.
- It must fit into the test section.
- The designed apparatus should not influence the characteristics of the oncoming air stream, i.e. it must not inhibit the free flow of the air from the tunnel.
- The apparatus must allow free flow of air around the model.
- The design has to allow for yaw conditions to be simulated and tested up to 15 degrees.
- The conveyor belt that produces the moving ground must be capable of speeds up to 80 km/h, or 22,22m/s.
- The entire system must be solid and free of vibrations.
- Provision must be made for a three component balance to be mounted on top of the rotating platform, so that the drag in the direction of the vehicle axis can be measured.
- This balance must be removed after each session.
- In front of the conveyor belt the oncoming boundary layer must be removed.
- A moveable probe should be mounted on the rotating platform to evaluate the air stream at several positions above and along the moving ground.

The structure should be built from 40 by 40 by 1.6 mm square tubing, All parts will be welded together. The support pads for the rollers can be constructed from wood, as

long as the frames are made up from the above square tubing. Once built, the structure will be cleaned and painted.
The use of castors will ensure the easy rotation of the platform and manoeuvrability of the entire rig.

DESIGN

To eliminate the relative velocities between the air stream and the ground that give rise to the formation of the boundary layer, a conveyor belt system will be used. This will ensure an endless moving ground capable of travelling at any speed above which the experiments can be carried out.

The design is characterised by a rotating platform, which carries the conveyor belt. The platform can be yawed at angles up to 15 degrees about its yaw axis. The three component balance is mounted on top of this platform and will thus measure the drag force experienced by the truck along its axis of symmetry. Components of this drag force will also yield the wind axis drag as experienced by the truck. Mounted on top of the platform is a sleigh, which carries the probe that will measure various characteristics of the air flow.

The model is mounted from above and kept in place by the balance. Provision is made for the balance to be positioned at any place across the width of the belt, to ensure complete use of the air stream.

Final positioning of the motor and gearbox units are not shown as specs from the manufacturers and suppliers were not available. Enough space is provided on the

sides of the platform unit for the mounting of these parts.

The rollers for the conveyor belt should have a radius of about 75mm and be tapered and rubberised. This will prevent the belt from running to one side and loosing grip at high velocities.

The motor and gearbox unit should deliver about 2850 rpm. Further, the motor should be speed controlled, so that the belt speed can be matched accurately to the air speed.

The following paragraphs will offer explanatory notes for all the drawings for the apparatus.

- *Figure A-1, Top View of Platform*
  This drawing was used to fix the boundaries and size of the belt and its supporting platform. The blue lines indicate the entrance and exit portions of the air stream onto the belt and thus indicate the confines that the apparatus must operate in. The two rollers are clearly marked by the dashed lines at either end of the platform. To ensure a smooth transition from fixed to moving ground, a circle of radius 1350mm is used at the transition point. The rectangle at the centre of the belt depicts the position of the model. The small circle within the right hand roller shows the yaw axis of the platform.

- *Figure A-2, Plan view of Platform at 15 degrees yaw.*
  The entire platform is rotated by 15 degrees. This will allow the evaluation of the drag coefficient at yaw. The model and balance can be moved along the width of the belt to allow optimum use of the air stream.

- *Figure A-4, Plan View of Rotational Positions of Platform*
  This drawing shows the platform at 0 degrees yaw (solid black lines) and 15 degrees yaw (dashed red lines). The purpose of this drawing is to determine the location of the rollers on the platform and alternatively the location and size of the support structures for the rollers on the base.

- *Figure A-3, Plan View of Platform with Critical Dimensions*
  All the important dimensions for the platform are supplied here. The section of the circle in the front that ensures the smooth linking to the wind tunnel will probably be perforated and be fitted with suction. This however will only be determined once the system is running.

- *Figure A-5, Plan View of the Base with Rotational Contacts*
  This drawing shows the base with the contact pads for the rollers of the platform. Also visible is the yaw axis and the entrance and exit points of the wind tunnel.

- *Figure A-11, Side View of Assembly*
  This drawing shows the entire structure, base and platform. It can be seen that the platform rests on the rollers and is rotated around its yaw axis. This rotational motion can either be done by a hand wheel and a set of bevel gears or a simpler and cheaper way would be to rotate the platform by hand around the fixed point.
  Also shown is the conveyor belt with its two rollers and the belt tensioner. The structure above the belt will carry the three - axis balance and the sleigh with the probe.

- *Figure A-12, Front View of Platform with Critical Dimensions*
  The details and critical dimensions of the rotating platform are shown in this drawing. The conveyor belt runs horizontally over a flat plate. The details for the

belt tensioner are not shown in this drawing. Also, the possible location and design of the suction box are also not shown.

- *Figure A-10, Front View of Base Assembly*
  The base of the assembly is shown here. The hand wheel used for yawing the platform through 15 degrees is also shown. As explained, an easier way would be to locate the platform at the yaw axis and turn it by hand. The structure must fulfil the requirement of mobility, this means that wheels or rollers need to be fitted to the base. When the apparatus is in use, these rollers must be clamped or locked so that the system cannot move.

- *Figure A-7, Side View of Assembly at Yaw, rhs*
  This is the drawing of the assembly looking from the right hand side. The dotted blue lines represent the exit of the wind tunnel. The dotted red lines show the position of the platform after being yawed by 15 degrees. The structure above the conveyor belt will support the balance and the probe.

- *Figure A-6, Side view of Assembly, RHS*
  This drawing shows the critical dimensions for the previous drawing. The height of the belt above the ground and the location of the yaw axis are the critical dimensions here.

- *Figure A-9, Side View of Platform, rhs*
  This drawing shows the platform viewed from the right hand side of the structure with the associated critical dimensions. The protruding part at the bottom of the platform is the flange that will allow the platform to be rotated about its yaw axis.

- *Figure A-8, Side View of Base, rhs*
  This is the side view of the base structure with all the critical dimensions.

REMOVAL OF THE BOUNDARY THROUGH SUCTION

This section is divided into the following sub sections that deal with each aspect of the suction in particular.

- Design and description of Apparatus
- Performance evaluation

The final effect that the removal of the boundary layer has on the drag properties of a bluff body in ground proximity will be discussed in the next section.

Design and Description of the Suction Apparatus

The same design criteria apply as in the previous section.

The suction apparatus is a box, which features a perforated top. At the sides of the box are the suction pipes, 25,4mm diam., which are connected to two powerful fans. The air is thus sucked through the perforated top of the box into the centrifugal fans.

The top of this suction box is the surface above which the model rests. This surface is completely flat and reinforced with aluminium struts on the inside of the box. This was learned during testing to be very important because the lower pressure in the box would result in the surface buckling under the pressure difference. The pattern for the suction holes was determined experimentally, as no satisfactory pattern could be found in the literature research.

Various patterns and hole sizes were experimented with, until a design was finally found that was acceptable. The surface is made up of five 1 mm thick galvanised steel sheets, all with the same length and width. This made the drilling on the NC machine easier and quicker, as all five sheets were clamped together and drilled at once. After drilling, the sheets were cleaned with a belt sander on both sides to remove the burrs from the drilling operation. Care was taken to use the belt grinder in such a way that the minute grooves introduced by the sander would not traverse the airflow, but rather that the air would flow along these grooves. Fig 2.1 shows the pattern employed on this suction surface.

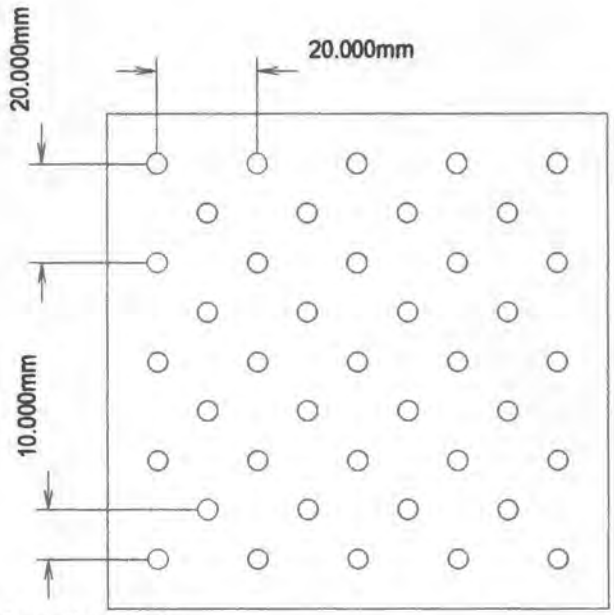

Fig. 2.1: Arrangement of suction Holes

Two types of suction are used to remove the boundary layer. Over the first 100mm of surface, a type of basic suction is used which removes the boundary layer that has formed on the nose and forward sections of the perforated surface. This section of basic suction is characterised by the same hole pattern as above, but differs in the size of the suction holes. To remove the larger boundary layer that has already formed, 5 mm diam. holes were drilled into this section. Larger holes could not be used, because this drastically reduced the suction velocity. The rest of the surface used distributed suction, which means that only the boundary layer that would build up over the 16mm between the holes had to be removed. The holes were 4mm in diam.

The distance between each hole in the above drawing is 20mm from centre to centre.

Figure B-5 in Appendix B shows the layout of the suction surface, with the 7 test locations and the suction pipes all clearly shown.

The front of the box is fitted with a large boundary layer scoop. This device removes the oncoming boundary layer already present on the wind tunnel floor. Also, due to the requirement of the balance being below the model, the surface of the suction floor had to be elevated to accommodate the three component balance below it. The height of the suction box could also not be made too small, as a uniform suction was required over the length of the test section. Reducing the height of the suction box would introduce local sections of a higher suction rate than experienced elsewhere.
The nose of the surface was shaped so as to produce a minimum oncoming boundary layer. Simply having a blunt end would result in a separated boundary layer, which would be very difficult to remove.

The sides of the suction floor were fitted with fences 40mm high. This was done to reduce the chance of any air being sucked in from the sides.

The entire suction box was mounted on a frame. This frame was in turn fitted with castors that could rotate and be locked in place. This allowed the entire apparatus to be removed and when in place, the brakes on the castors ensured that the apparatus did not move on the ground.
Along the top of the frame a sledge was mounted that allowed the probe to be moved along the length of the test section (x-direction), the width of the test section (y-direction) and the height of the test section (z-direction). This moveable probe was vital in surveying the test section to ensure a high quality air stream.

The end of the pitot tube used to measure the stagnation pressure was fitted with a contact indicator light. This means that when the probe touched the surface, a current would flow and an LED would light up. This was vital to determine when the probe touched the ground, as deflection of the stagnation pressure measuring probe could damage it.

Test points are located at certain intervals along the x-axis. These locations are identified in the table below. The points are measured from the leading edge of the suction box.

Test Point	***Location (mm)***	***Significance***
1	85	
2	165	
3	245	Front of model
4	480	
5	780	Model midpoint
6	1075	
7	1315	Model endpoint

Certain sections of the suction floor to the side of the model were blocked off from the suction. This was done because at high velocities, the wind tunnel started to resonate, producing a high pitched and very irritating noise. Further, by covering up sections that did not require boundary layer removal, the available suction could be used to improve the suction rate in the more important areas. This was seen to reduce the boundary layer thickness by about 20% in front of the model

Appendix B shows all the relevant drawings of the above device.

Figure B-1

This drawing is a front view of the support structure carrying the suction box. The castors that allow the entire apparatus to be moved are all clearly visible. The suction box will rest on the three cross bars which in turn are welded onto the main horizontal structure bar.

Figure B-2

This drawing is a side view of the support structure. To facilitate easy movement, the lower horizontal support bar on the right hand side is removed so that the structure can be moved around the three component balance, which is resting on the floor.

Figure B-3

This drawing shows the top and the side view of the suction box. As mentioned before, the reason for the large boundary scoop is to lift the suction box so that the three axis balance fits below it. The entire box is made from 1mm galvanised sheet metal which is bent and then riveted together. All gaps and joints are sealed with a silicon component. Sealing improves the suction at the suction holes.

Figure B-4

This drawing shows a 1:1 view of the forward section. This section contains the nose part, which is shaped so as to keep the boundary layer to a minimum. The base of this nose is made from nylon, the sheet metal being fitted into the material and a round steel bar with a 4mm diameter being fitted directly onto the front section, to give a perfectly round cross section.

Figure B-5

This drawing shows all the test points at which boundary layer thickness measurements are taken. Point 3 is the foremost point of the model and point 5 is the mid section of the truck model. The sting from the three axis balance is attached to the model at this point.

This point will be referred to in later sections of this thesis with a t subscript.

Performance Evaluation

This section of the thesis deals with the performance evaluation of the suction apparatus. This is done by determining the quality of the air stream by analysing key performance indicators.

- Wind Tunnel Description
- Pitot Tube Calibration
- Suction Calibration
- Boundary Layer Thickness and Displacement Boundary Layer Thickness
- Static Pressure Gradient
- Dynamic Pressure Distribution

WIND TUNNEL DESCRIPTION

The wind tunnel that was used for all the experiments is of a single return open jet type located at the University of Cape Town Mechanical Engineering Department. The wind tunnel offers a maximum tunnel speed of about 35m/s. The speed is adjustable via a rotating knob on the control panel, which regulates the pressure in front of the fan. The maximum volume flow rate is about 13.5m^3/s, and the contraction ratio is 10:1.

PITOT TUBE CALIBRATION

All measurements relating to the flow quality will be done by examining the total and static pressures and the difference between the two at any point in the flow. The difference in pressure will be used to determine the local flow velocity by using the Bernoulli Equation.

$$v^2 = \frac{2\Delta P}{\rho} \qquad 2.1$$

However, due to the requirement that thin boundary layers had to be examined, a new pitot tube was constructed. This new pitot tube was smaller than existing models in the department and could thus be used to analyse the flow close to the ground without influencing the flow.

The new pitot tube was made from a hypodermic needle, 45mm long. The needle was heated and the last 10mm were bent at 90 degrees to the remaining needle.

This small pitot tube could now be used to measure the total pressure very close to the ground. First the new pitot tube had to calibrated.

The static pressure was measured with a standard pitot tube in the same vertical plane but well above the ground floor. The difference between this static pressure and the stagnation pressure recorded by the pitot tube is used to evaluate the flow velocity at any local point that the stagnation pressure is measured at.
This combination of standard and non - standard pitot tube is calibrated against a standard pitot tube. The pressure difference on the standard pitot tube is measured with an inclined alcohol manometer and is registered in millimetres of inclined alcohol. Through the following equation, this column of alcohol is converted to an actual velocity reading.

$$v^2 = \frac{2SFx}{\rho} \qquad 2.2$$

- SF: This factor depends on the inclination of the manometer
- x: This is the length of the column of alcohol in millimetres
- ρ: This is the density of the fluid.

The velocity from the combination of pitot tubes is calculated from the difference in pressure between the two pitot tubes (Equation 2.1). These two pitot tubes are connected to a digital manometer, which will register the pressure difference in Pascals.
For each wind speed, the pressure difference and actual flow velocity are recorded and plotted as actual flow velocity (v_a) versus Δp as recorded on the combination pitot tube (fig 2.2).

Further, the measured velocity from the combination of pitot tubes is plotted against the actual velocity obtained from the standard pitot tube (fig 2.3).

This plot is used to derive a relationship between the actual flow velocity and the measured flow velocity. Here v_m with a subscript m is referring to the velocity measured by the combination of pitot tubes.

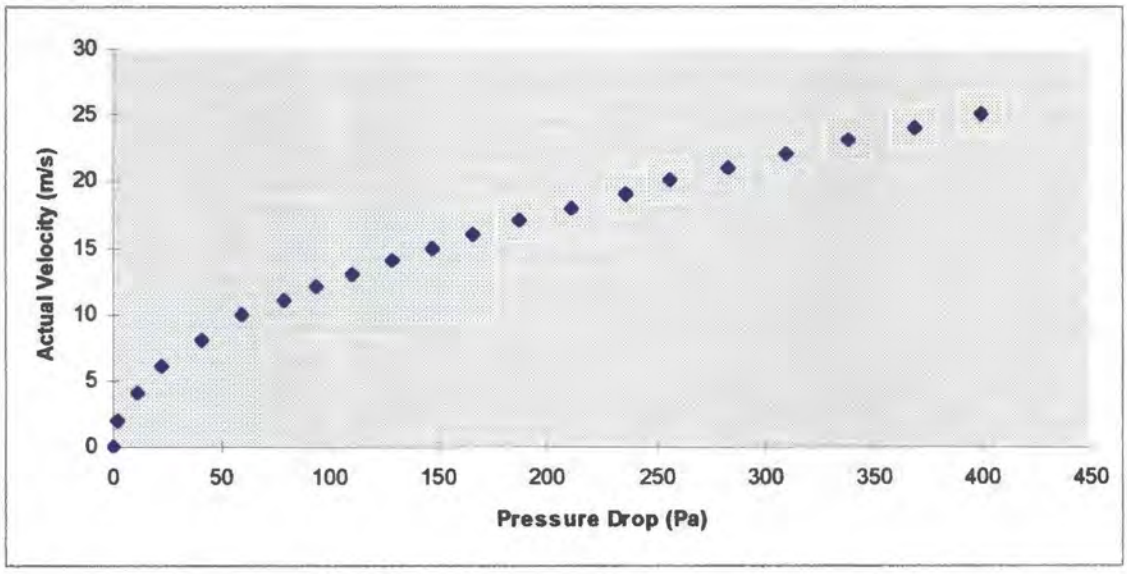

Fig. 2.2: Actual Velocity versus Pressure Drop

Below in fig 2.3 the linear relationship between actual and measured flow velocity is obvious.

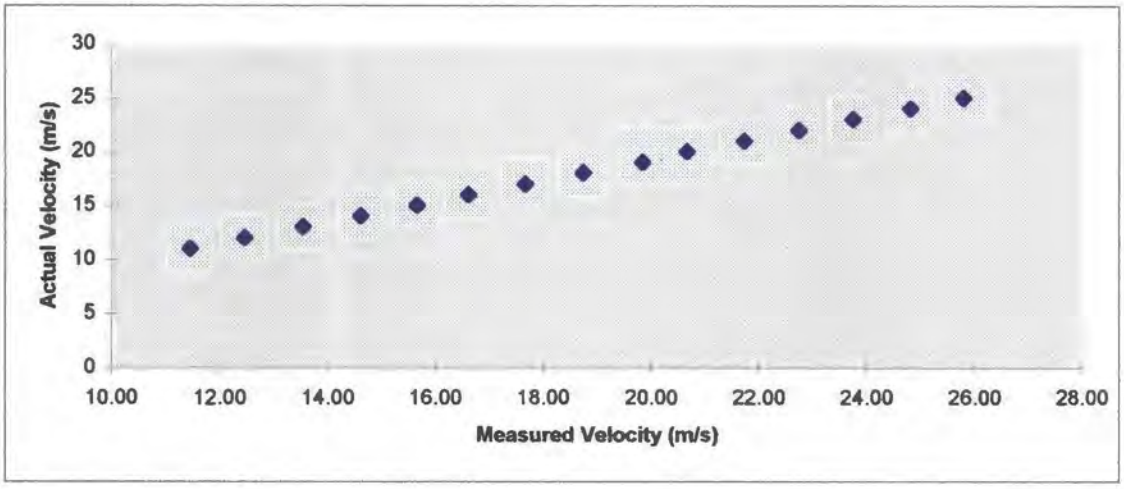

Fig. 2.3: Actual Velocity versus Measured Velocity

The above graph is mathematically represented by equation 2.3.

$$v_a = 0.9637 v_m + 0.0413 \qquad 2.3$$

Solving equation 2.1 for v_r and inserting this equation into equation 2.3 will yield a relationship between the actual flow velocity and the registered pressure difference across the standard pitot tube used to measure static pressure and the non standard pitot tube measuring stagnation pressure.

$$v_a = 1.244\sqrt{\Delta P} + 0.0413 \qquad 2.4$$

Or

$$\Delta P = \left(\frac{v_a - 0.0413}{1.244}\right)^2 \qquad 2.5$$

With the use of the two above equations relating the actual flow velocity at a point to the pressure difference at that point, any flow velocity or pressure difference can be calculated.

SUCTION CALIBRATION

This section deals with the correct suction being applied to the suction surface. Two fans were connected to the suction box. Table 2.1 indicates the most important feature of each fan.

	Fan 1	Fan 2
Type	Centrifugal	Centrifugal
Flow rate	Fixed	Varied
Impeller Size	840mm	510mm
Inlet Ports	5	5
Maximum Flow rate (m^3/s)	0.078	0.124
Maximum Discharge Velocity (m/s)	61.80	58.24

Previous investigations had revealed that many bluff bodies are not sensitive to over-suction. However, no detailed description of these bluff bodies was given and it was felt that the vertical velocity imposed on the body by the suction might influence readings, especially the lift force experienced by the body.

It was thus felt that the suction should be calibrated so that the correct amount of boundary layer air was removed at a certain speed. This was done by moving the probe to point 3, 4mm in front of a suction hole with the probe touching the floor. The air speed was set and the pressure drop recorded. The pressure drop was recorded for maximum suction, i.e. the butterfly valve on fan 2 fully open. The butterfly valve was then slowly closed and the flow rate through fan 2 slowly decreased until the pressure drop across the pitot tubes was dropping. This would indicate that as the valve was closed, not enough of the retarded air was sucked away and the speed of the air flow close to the ground was dropping. This procedure was repeated for wind speeds from 10 m/s to 24 m/s at intervals of 2 m/s.

For each setting of the valve, the velocity distribution across the outlet of fan 2 was determined with the aid of a standard pitot tube and a digital manometer. The velocity was determined from the difference in pressure and integrated over the diameter of the outlet and finally divided by the number of readings. This method would result in an accurate average discharge velocity for each valve setting.

Summing the discharge flow from fan 1 and fan 2 for each speed setting of the wind tunnel resulted in the total suction rate for each wind speed setting in the tunnel.

At the same time, a theoretical approach was used to verify the experimental result. Referring to Fig. 2.1, it was reasoned that the boundary layer could grow for 16mm, until it was sucked off again. Using the equation for a laminar boundary layer growth (Reynolds number below 500000) the mass flow in the boundary layer can be found.

$$\frac{dM_{BL}}{dt} = \int_0^{\delta} \rho u dy \qquad 2.6$$

Knowing the velocity distribution across the boundary layer and the boundary layer thickness, the above can be evaluated. In a laminar boundary layer, the velocity distribution is given by

$$\frac{u}{u_\infty} = 1.5\frac{y}{\delta} - 0.5\left(\frac{y}{\delta}\right)^3 \qquad 2.7$$

Inserting equation 2.7 into equation 2.6.

$$\frac{dM_{BL}}{dt} = \frac{5}{8}\rho u_\infty \delta \qquad 2.8$$

Equation 2.8 calculates the mass flow rate in the boundary over a unit width of 1 meter.

The boundary layer thickness in the laminar flow region at any x position is given by

$$\frac{\delta_x}{x} = 5\left(\frac{u_\infty x}{v}\right)^{-\frac{1}{2}} \qquad 2.9$$

The suction surface is now divided into sections of 100mm by 100mm. Each section contains 50 suction holes. Assuming that each hole has to suck off the boundary layer forming on the area directly in front of it, the required suction rate can be calculated.

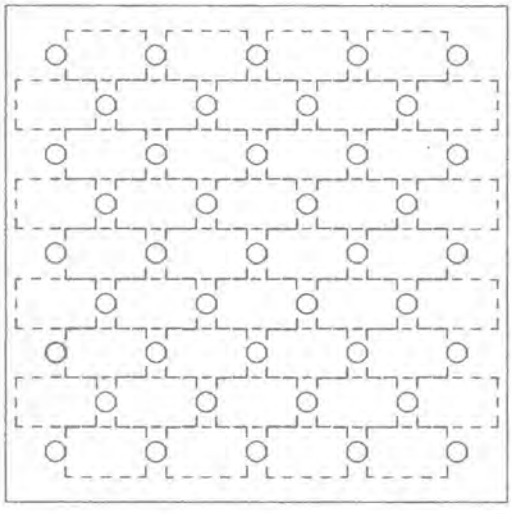

Fig. 2.4: 100 by 100 suction section with suction holes

Each of the above sections has 50 such patches. Thus equation 2.8 can be modified to first calculate the mass flow rate in the boundary layer for each patch and then summing the 50 patches per section will give the total boundary layer that has to be sucked off over the 100mm by 100mm.

Per patch, equation 2.8 becomes

$$\frac{dm_{bl}}{dt} = \frac{5}{800}\rho u_{\infty}\delta \qquad 2.10$$

Per 100 by 100 suction section, equation 2.10 is multiplied by a factor of 50.

$$\sum \frac{dm_{bl}}{dt} = 0.3125 \rho u_{\infty} \delta \qquad 2.11$$

The total suction area has 64 such sections. Multiplying equation 2.11 by a factor of 64.

$$\sum \frac{dm_{bl}}{dt} = 20.08 \rho u_{\infty} \delta_{16} \qquad 2.12$$

Equation 2.12 calculates the required suction for the distributed suction area. This is also indicated by the sub-script 16 , which is the distance between each hole, for the boundary layer thickness.
For the basic suction, equation 2.11 is used and multiplied by a factor of 6.

$$\sum \frac{dm_{bl}}{dt} = 1.875 \rho u_{\infty} \delta_{15} \qquad 2.13$$

The subsripts denote that one hole has to suck off the boundary layer forming over 15mm and the other hole has to suck off the boundary layer forming over 16mm.

The total volume of air that has to be removed can then calculated as

$$\frac{dV_{BL}}{dt} = u_{\infty}(1.875\delta_{15} + 20.08\delta_{16}) \qquad 2.14$$

Fig 2.5 is a plot of the theoretical (Qt) and actual (Qf) boundary layer flow rates as determined by the suction of the air versus tunnel wind speed. The graphs correlate well and only show a slight divergence at tunnel wind speeds over 18m/s. This is caused by the fact that the available suction is insufficient for the boundary layer flow rate. Fig. 2.6 is a plot of the mean suction velocity versus the tunnel wind speed. This velocity is defined as the suction flow rate divided the suction area. Again the theoretical and actual values are compared.

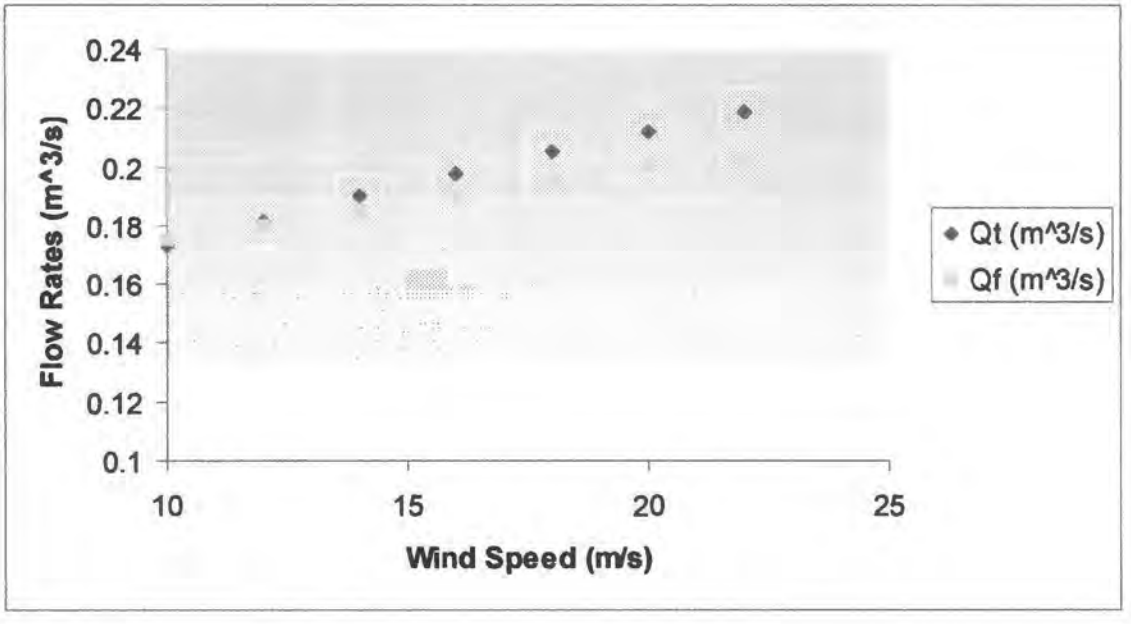

Fig. 2.5: Actual and Theoretical boundary Layer Flow Rates

Fig 2.7 is a plot of the velocity ratio versus the tunnel wind speed. The velocity ratio is defined as the mean suction velocity divided by the tunnel wind speed. This ratio is used in modern wind tunnels to compare results and it is vital that this value be kept to a minimum to prevent over-suction.

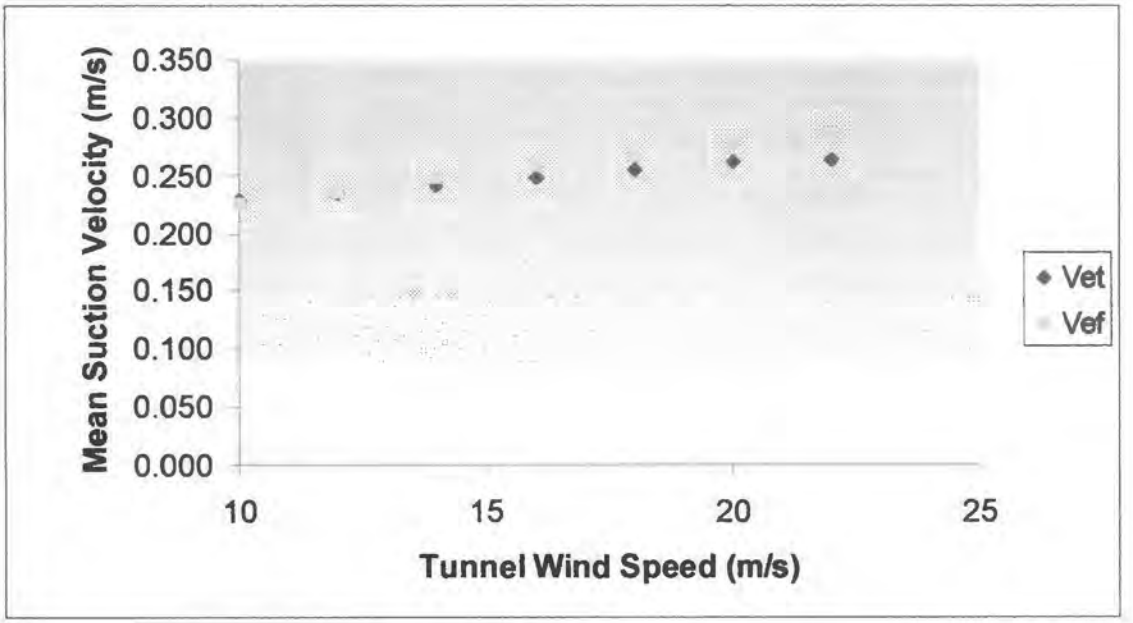

Fig. 2.6: Actual (Vef) and Theoretical (Vet) Suction Velocities versus Wind Speed.

The two plots in fig 2.6 correlate again very well until the higher tunnel wind speeds are reached.

The next plot, fig 2.7, clearly shows a downward trend with increasing tunnel velocity. This is partly due to the fact that the thickness of the boundary layer decreases as the wind tunnel speed increases.

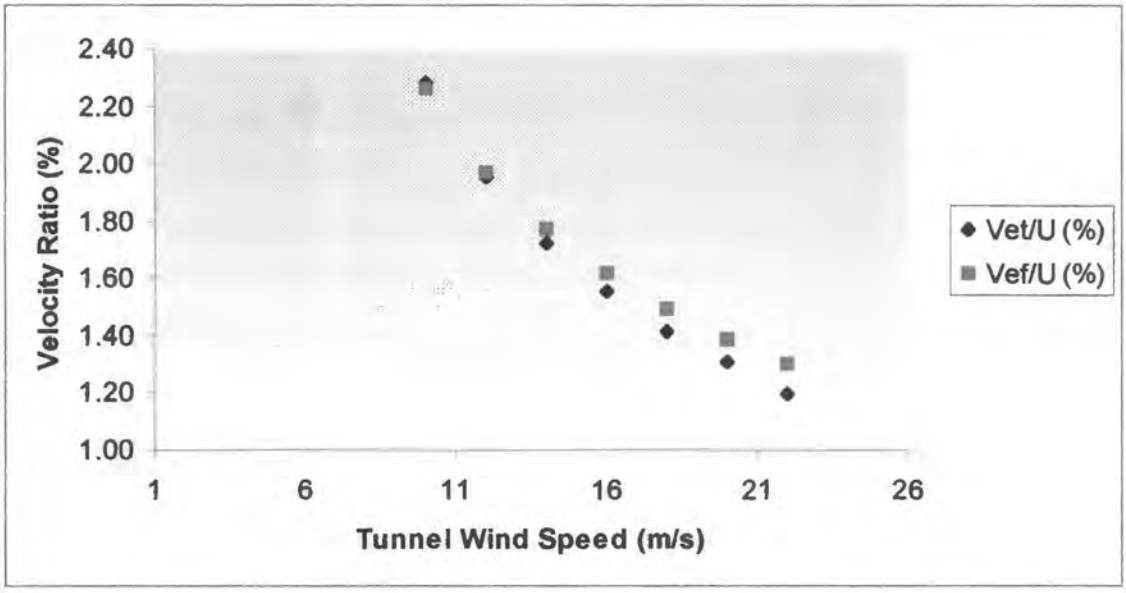

Fig. 2.7: Actual (Vef/U) and Theoretical (Vet/U) Velocity Ratios versus Wind Speed.

BOUNDARY LAYER THICKNESS AND DISPLACEMENT THICKNESS

In this section the boundary layer thickness is measured at all test locations. This is done by moving the probe from the surface along the y-axis and noting the pressure difference. Using equation 2.4, this pressure difference is converted to a velocity. This information is then plotted as the non-dimensional (v/v_s) velocity against the height above the surface.

At each location the boundary layer displacement thickness is also evaluated. This is an important parameter when considering this type of flow because it directly indicates how much less air is flowing in the boundary layer region by lifting the floor by the boundary layer displacement thickness. The boundary layer displacement thickness is evaluated as follows.

$$\delta^* = \int_0^{\delta} \left(1 - \frac{v}{v_s}\right) dy \qquad 2.15$$

The importance of plotting the non-dimensional velocity becomes clear now. By using numeric integration, i.e. by using Simpson's 1/3 Rule, equation 2.15 can be evaluated as follows

$$\delta^* = \delta - \int_0^{\delta} \left(\frac{v}{v_s}\right) dy \qquad 2.16$$

These calculations are performed for each test point with the suction on and off. The curves are compared and the improvement is calculated.
The results of this survey are shown in the following graphs. The free stream velocity was kept constant at 22.2 m/s.

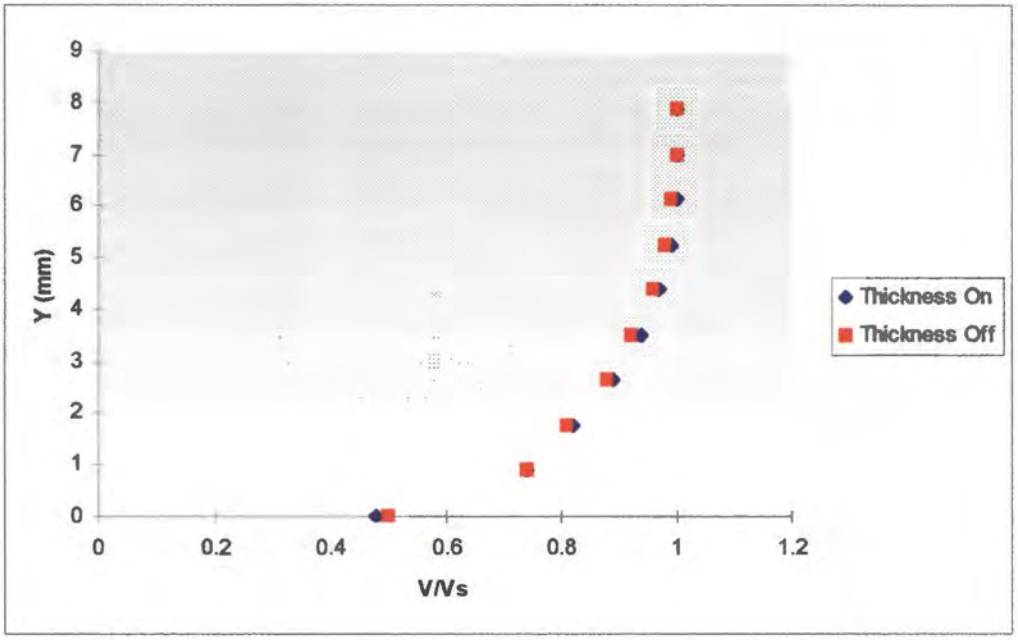

Fig. 2.8: Boundary Layers at Station 1

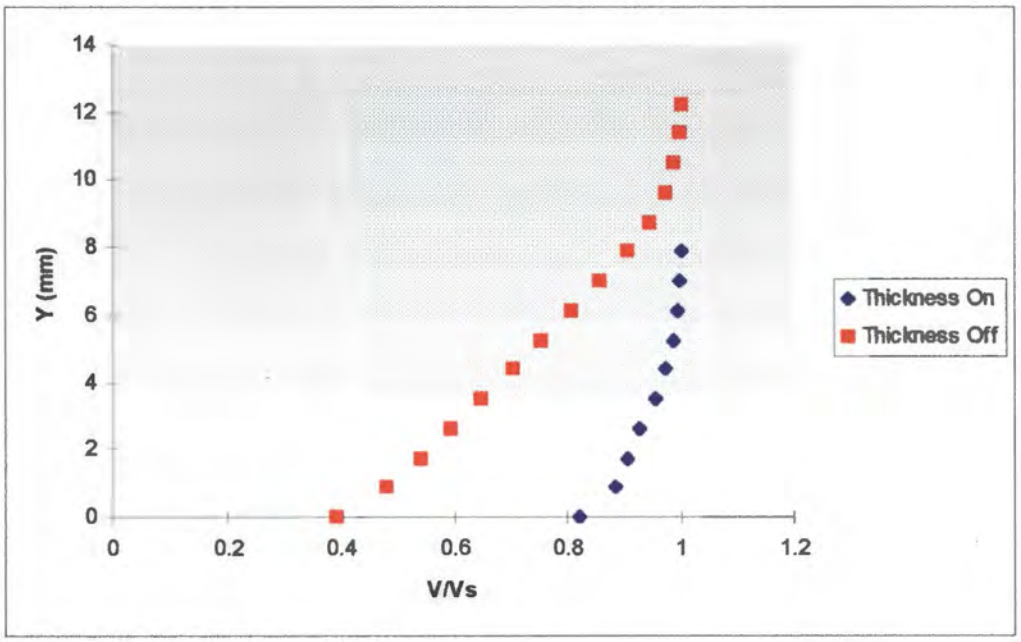

Fig. 2.9: Boundary Layers at Station 2.

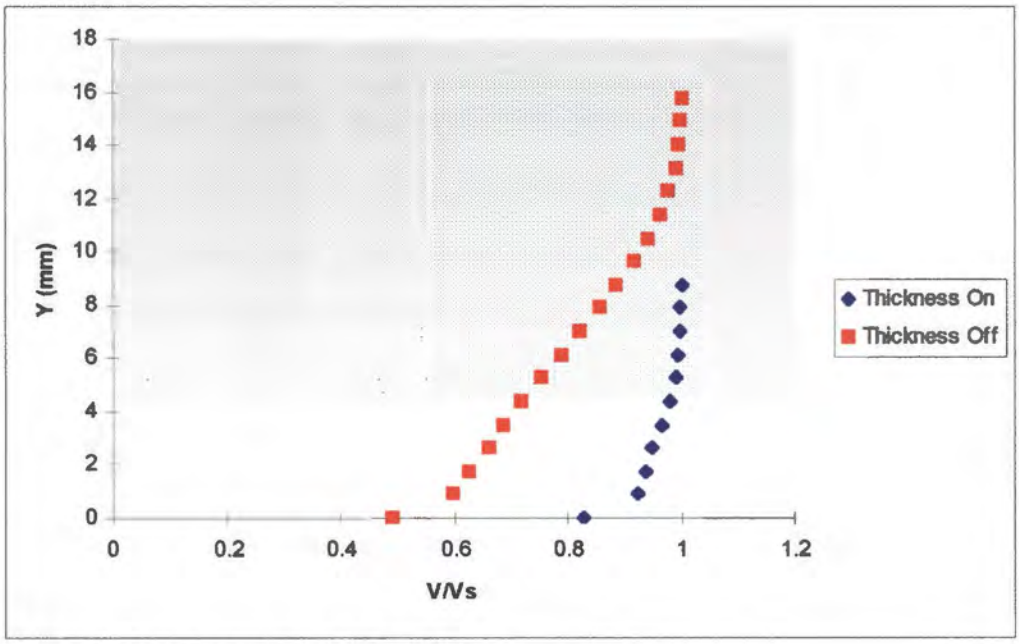

Fig. 2.10: Boundary Layers at Station 3.

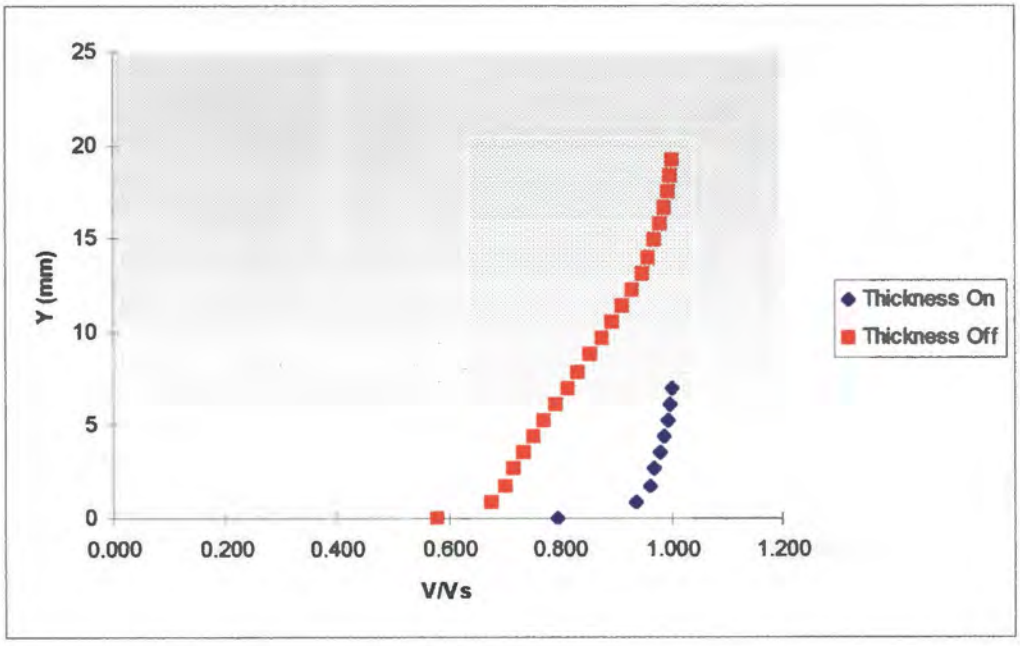

Fig 2.11: Boundary Layers at Station 4.

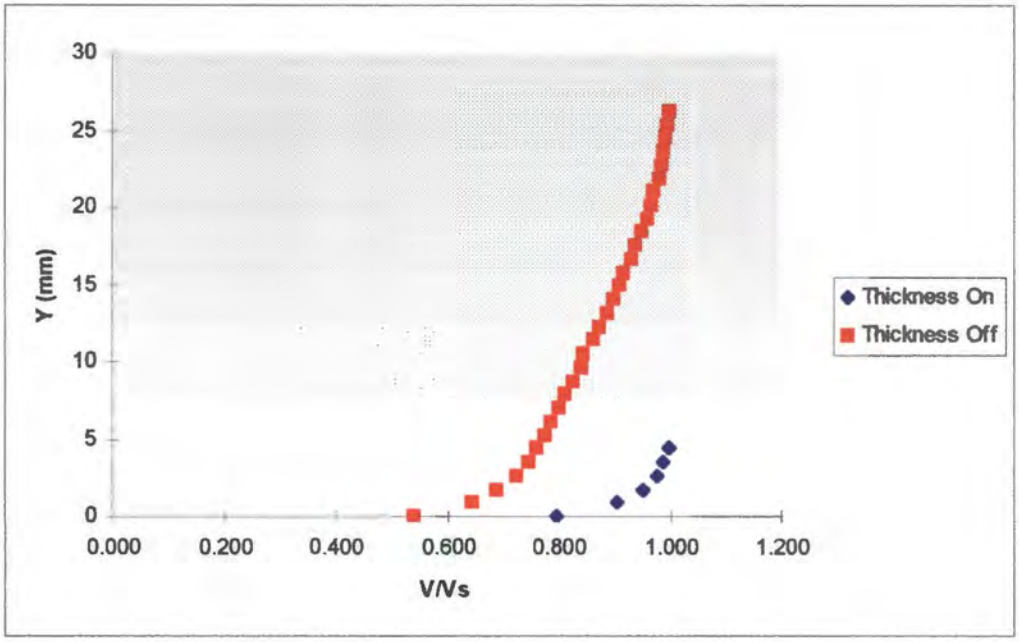

Fig. 2.12: Boundary Layers at Station 5.

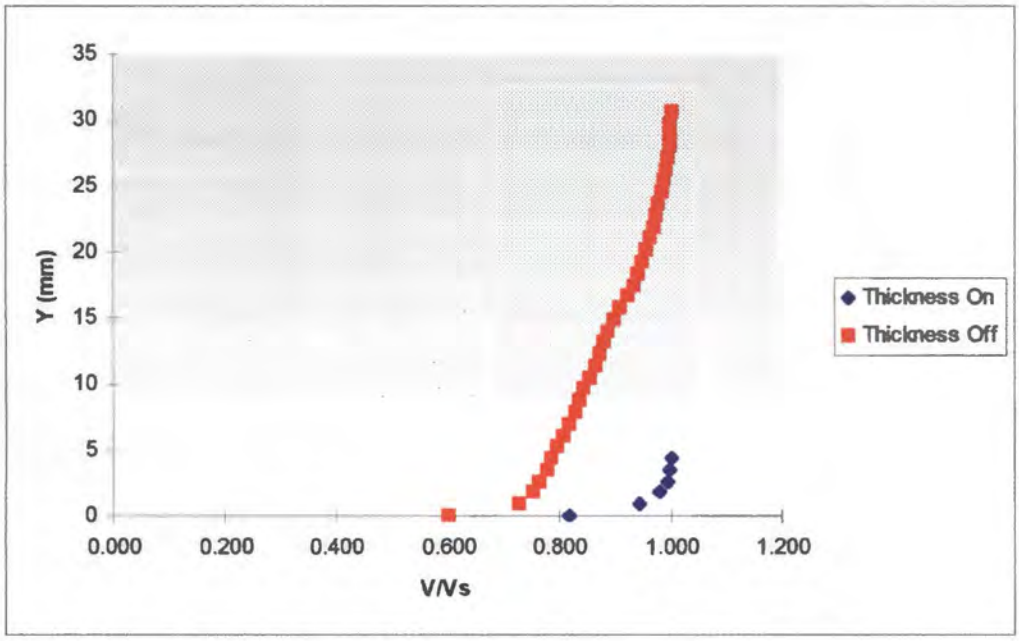

Fig. 2.13: Boundary Layers at Station 6.

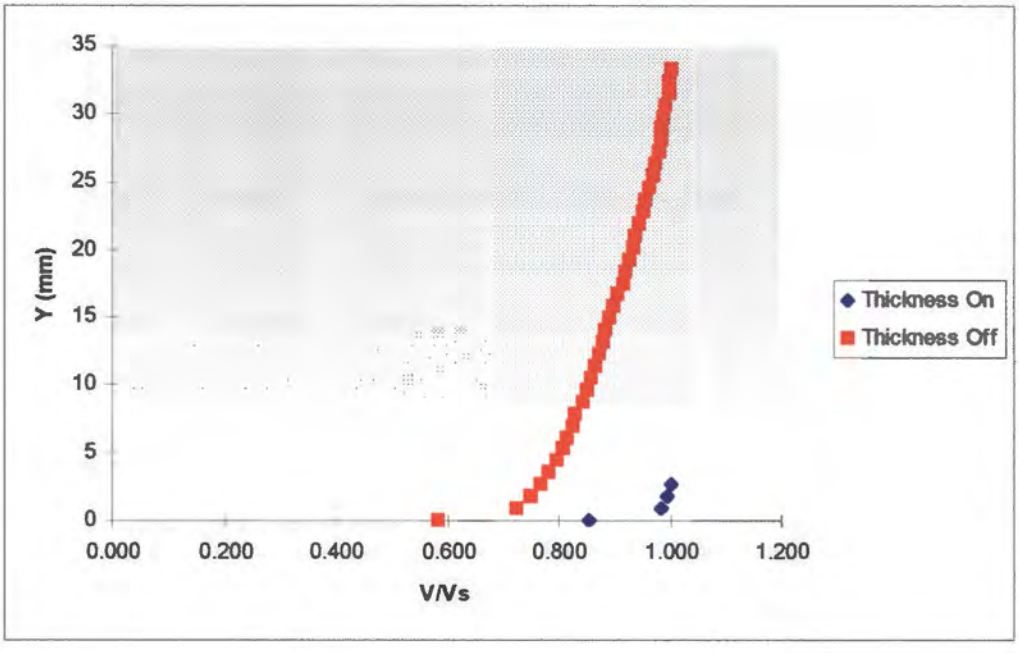

Fig. 2.14: Boundary Layers at Station 7.

The following two graphs summarise the state of the boundary layers over the test section length.

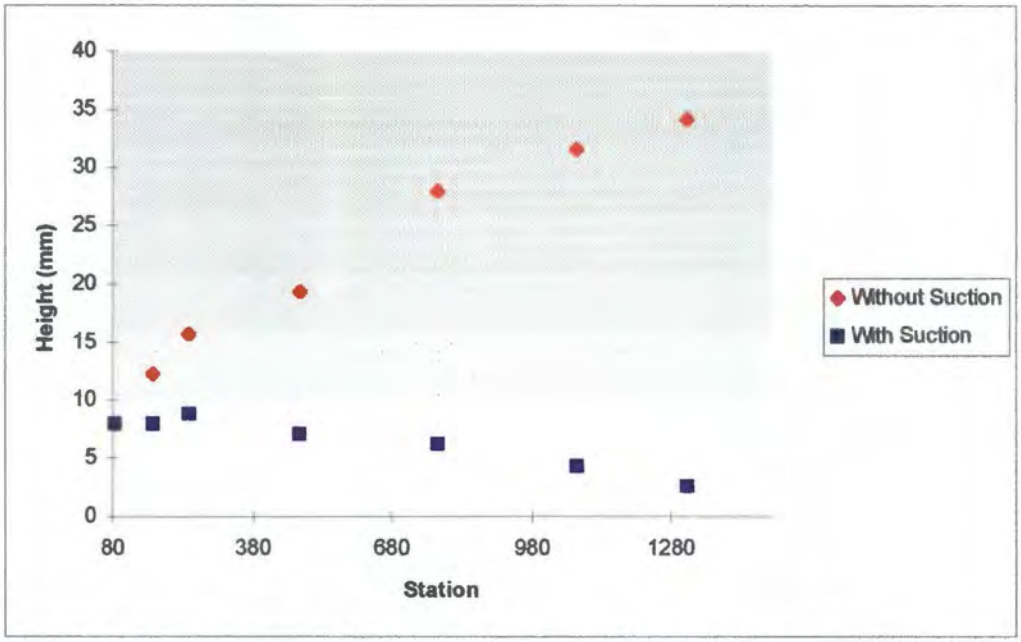

Fig. 2.15: Boundary Layer Thickness versus Test Section Length

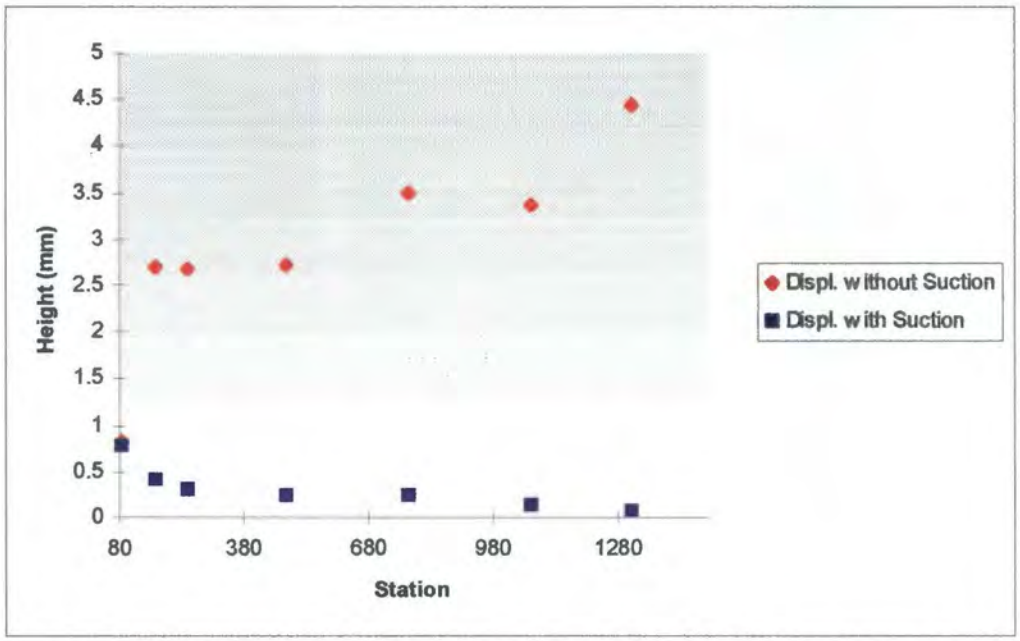

Fig. 2.16: Boundary Layer Displacement Thickness versus Test Section Length

The table below shows the boundary layer thickness, boundary layer displacement thickness.

Test Location	Suction On δ (mm)	Suction Off δ (mm)	Suction On δ^* (mm)	Suction Off δ^* (mm)
1	7.88	7.88	0.77	0.82
2	7.88	12.25	0.4	2.7
3	8.75	15.75	0.3	2.67
4	7	19.25	0.23	2.72
5	6.13	28	0.24	3.5
6	4.38	31.5	0.14	3.36
7	2.56	34.13	0.07	4.43

A reduction of 44% in boundary layer thickness and 89% reduction for the boundary layer displacement thickness is observed for station 3, i.e. at the front of the truck model.

DYNAMIC REFERENCE PRESSURE[19]

This section is not vital to the evaluation of the suction device, but certain ideas will become useful in the following sections. It was thus felt that the topic should be introduced at this point.

The determination of the reference dynamic pressure or reference velocity is of fundamental importance, because it is a reference quantity for all dimensionless force and moment coefficients of a test object. The ΔP – Nozzle method measures the average velocity in terms of the static pressure difference between two sections within the nozzle. The first one is in the settling chamber and the second is before the nozzle exit. However, the static pressure close to the nozzle exit is influenced strongly by the model in the test section and can thus not be used to accurately determine the correct dynamic reference pressure. This is caused by the loss in mass flow rate due to the model blocking off some of the airflow.

To counter this problem, a tunnel factor is introduced. At first, the point in the nozzle is selected so that the presence of the model will not influence the static pressure reading. It was found that for the long truck model, this point lay 1.5 model lengths upstream of the front of the model. The difference in static pressures between this point and the settling chamber was then measured for each flow velocity. At the same time the dynamic pressure at the test section central location was measured. This procedure was carried out in an empty tunnel.

The above data is then inserted into the equation below and the tunnel factor determined finally.

$$Q_T = K_{WT}(P_S - P_N) \qquad 2.17$$

- Q_T Dynamic Pressure at test section central location.
- P_S Static Wall Pressure in settling chamber.
- P_N Static Wall Pressure in the nozzle.
- K_{WT} Tunnel Factor, =2.76

Alternatively, a graph of Q_T versus ($P_S - P_N$) is plotted (Fig. 2.17)

For later testing, the difference in static pressure in the nozzle is read off on the digital manometer and the above relation will indicate the correct dynamic reference pressure.

The graph below is a plot of the dynamic reference pressure versus the static pressure difference across the nozzle.

Alternatively, the following relationship is derived from the above plot.

$$Q_T = 2.785(P_S - P_N) + 0.196 \qquad 2.18$$

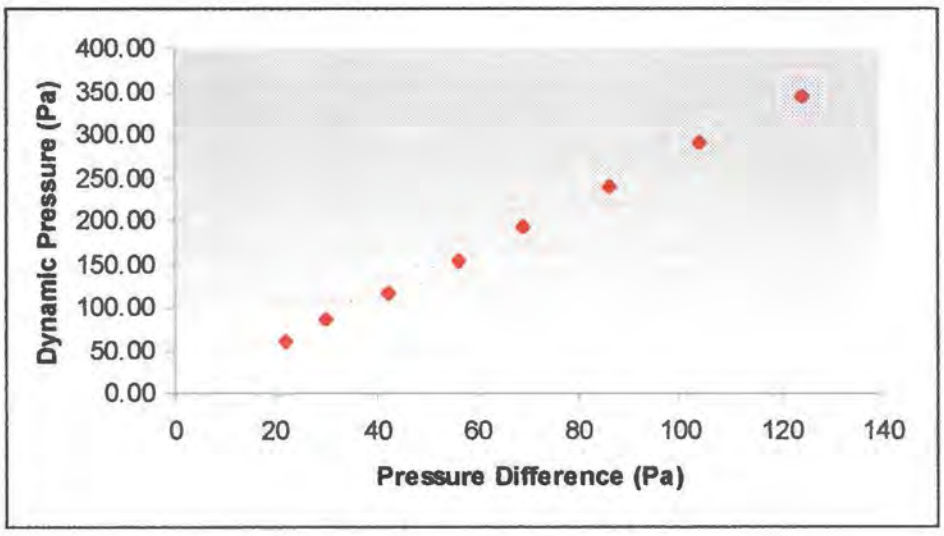

Fig. 2.17: Tunnel Factor Calibration Curve.

DYNAMIC PRESSURE UNIFORMITY

The primary indicator of flow quality is the test section dynamic pressure uniformity. Dynamic Pressure (q) surveys were made at the third test location, from z=-200mm to z=+200mm at 100mm intervals and from y=0 to 150mm at 14mm intervals.
The results obtained were then summed to arrive at an average dynamic pressure for that x-location ($\bar{q}$). The results were then plotted as

$$D_{PU} = 100\frac{q-\bar{q}}{\bar{q}} \qquad 2.19$$

The graph below is a plot of this data. Note that the boundary layer has been included in the plot.

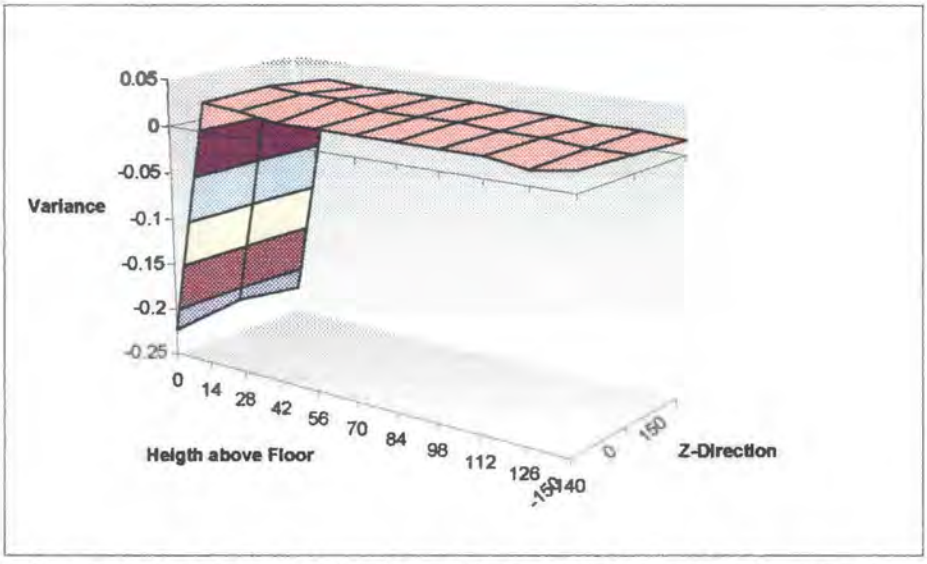

Fig. 2.18: Dynamic Pressure distribution at Front of Vehicle with BL present.

The following is a plot of the same data. This time, however, the boundary layer velocity distribution is not included.

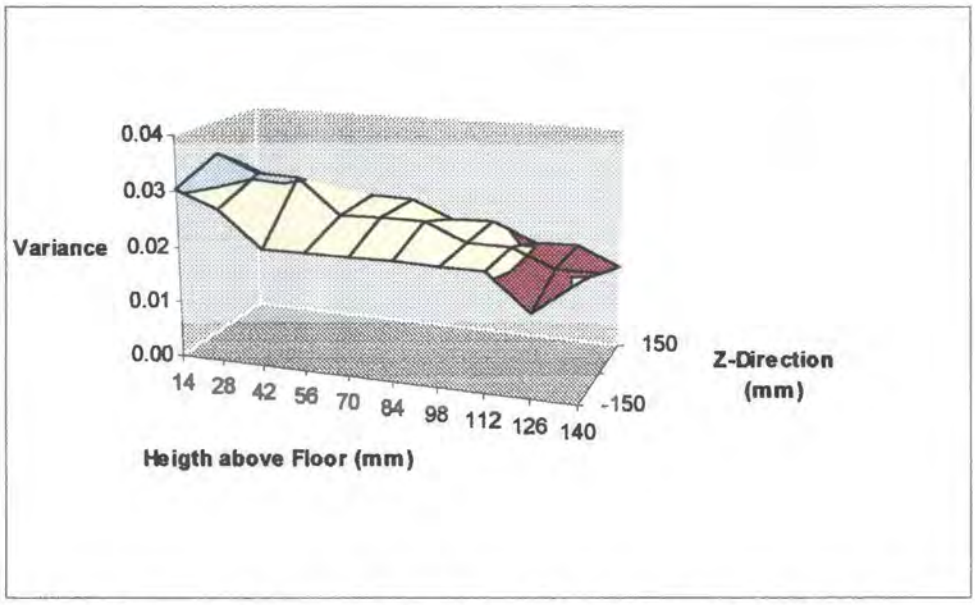

Fig. 2.19: Dynamic Pressure distribution at Front of Vehicle without BL present.

As can be seen from this plot, the scatter of the readings lie well within the allowed 5 percent of the mean value of the dynamic pressure.

STATIC PRESSURE COEFFICIENT[19]

The static pressure coefficient in a wind tunnel is defined as the change in static pressure divided by the dynamic pressure at the centre of the test section. This value should be as small as possible, because large coefficient values are caused by large changes in static pressure. This large static pressure change in turn will affect the drag and lift readings measured on the model in that the model will experience a changing lift force, due to a large difference in static pressure along its length. If this is the case, then the readings taken have to be corrected for this buoyancy effect.

The static pressure is measured with the standard pitot tube at each test location. However, due to the effect that the model has on the flow in the test section, a flow equivalent system has to be set up. This is done by introducing the static pressure on the walls of the settling chamber as a constant in the calculations. The static pressure acting on the walls experiences an increasing degree of influence as one travels along the nozzle towards the model. It was shown that the static pressure acting on the walls of the settling chamber is not influenced by a model being put into the wind tunnel test section, downstream of the settling chamber.

Traditionally, the static pressure coefficient is determined as

$$C_P = \frac{\Delta P}{Q} = \frac{P_I - P_U}{Q_T} \qquad 2.20$$

As mentioned above, the static settling chamber pressure (P_S) is introduced

$$C_P = \frac{P_I - P_S}{Q_T} - \frac{P_U - P_S}{Q_T} \qquad 2.21$$

The last term in the above equation is known as the Static Pressure Offset.

- P_l Local Static Pressure with model present.
- P_U Static Pressure of Undisturbed Flow at test section central point.
- Q_T Dynamic Pressure of undisturbed flow at test section central point as calculated in the previous section.

The following fig 2.20 is a plot of this data.

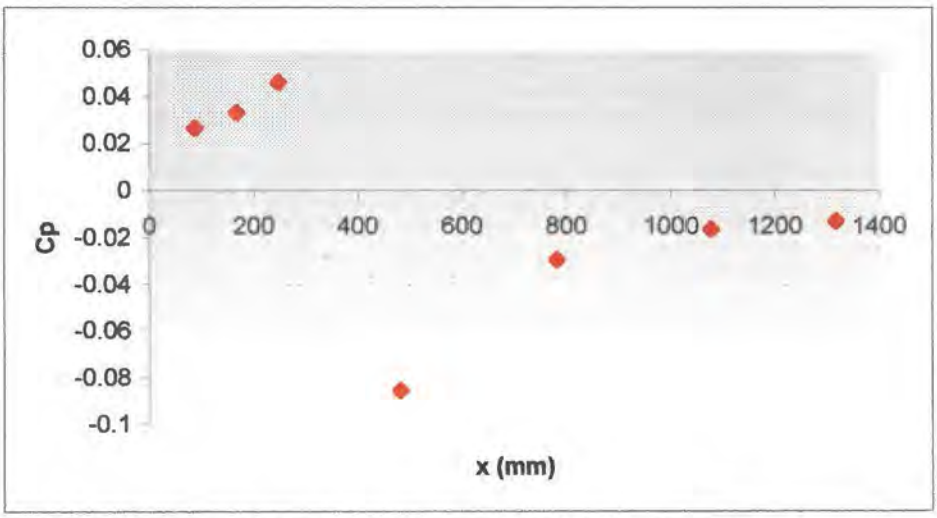

Fig. 2.20: Static Pressure Coefficient versus Test Section Length

Noticeable is the change in sign of this coefficient at about 340mm. This is due to the container – cab gap. This gap is known to dramatically influence the aerodynamic characteristics of large trucks, a fact that is shown here clearly[1]. Due to large turbulence produced by this gap, the average velocity increases rapidly with a resultant decrease in pressure.

The static pressure coefficient levels out again downstream of this gap.

MODEL DESCRIPTION

The model used in this research was a horse and trailer combination. The trailer is a 1/24 U.S. Refer Trailer made by ITALERI. The horse is a 1/24 FORD AEROMAX 120. The reason for choosing the Ford model as horse is that it is characterised by a very streamlined shape and high model detail. This aspect was found to be very important in the literature survey[2].

To facilitate rotating wheels, the two plastic model kits were placed onto an aluminium frame, essentially made up of two parallel running H-beams. These beams were held in place by separators running the entire length of the beams. The 5 axles were mounted onto this solid aluminium frame. The axle sub assemblies were complete units, i.e. two axles were joined before they were mounted onto the beams. This was obviously not required for the front axle, as it was single.

Once the sub axle assemblies were securely glued and bolted onto the aluminium H-beams, the plastic model casings were put in place. The plastic trailer base was glued and bolted into place. One side panel was then glued onto the base. The top section and other side panel were glued together and were bolted onto the base and side panel. This would allow access to the motor units running the twin axles. The motor units for the two twin axles assemblies were glued onto the trailer base and connected via belts to the pulley on the axle. The horse casing was glued together entirely and then bolted onto the front sections of the aluminium sub assembly. Again this would allow access to the motor unit running the front axle.

One common electrical connection point was constructed inside the model. This meant that all the electric cables for the motors would be found in one point.

The model was then painted. The photographs of the finished model are in Appendix C.

CHAPTER 4 – EXPERIMENTAL METHOD, MODEL TESTING

Various tests were conducted on the model in the wind tunnel to establish the influence that the boundary layer has on the aerodynamic drag of the model.

- *The Aerodynamic Drag is measured at various Ground Clearances*
- *The Drag Coefficient is computed at various Reynolds Numbers*
- *Aerodynamic Drag at different Yaw Angles*

Also, the model was subjected to various test simulations. These conditions are classified as Types 1 through 4.

- Type 1: *Suction Off, Rotation On.*
- Type 2: *Suction Off, Rotation Off.*
- Type 3: *Suction On, Rotation On.*
- Type 4: *Suction On, Rotation Off.*

The rotation refers to the rotation of the axles, and the suction to the removal of the boundary layer. Suction On means that the fans are switched, the correct flow rate is selected and the boundary layer is removed. Rotation On means that the axles are rotating. The rotational velocity of the wheels was measured at about 5500 rpm, or a ground speed of 45 km/h. It was not possible to achieve higher rotational speeds. The rotational speed was kept constant for all wind speeds. This was done by adjusting the voltage across each DC motor to 18 V for each series of tests.

An analysis of the above tests is performed each time to determine the influence of the boundary layer on the aerodynamic drag.

Some tests are also performed with a skirting on the truck.

The model is mounted above the suction surface via a sting to the three component wind tunnel balance. To facilitate this, a 35mm hole was drilled into the bottom and top surfaces of the suction box. The sting was then inserted through these two holes into the balance sitting below the suction box. Before testing commenced, the aerodynamic drag that the sting experienced without the model mounted was recorded at various heights of the sting top above the surface. It was found that the changes in drag were negligible for sting movements of a maximum of 25mm. 25mm is the maximum amount that the sting could be moved vertically without jeopardising the rigid clamping of the sting.

The following photograph shows the suction surface, with the sting protruding through it. The cables for the motors are fed through the sting.

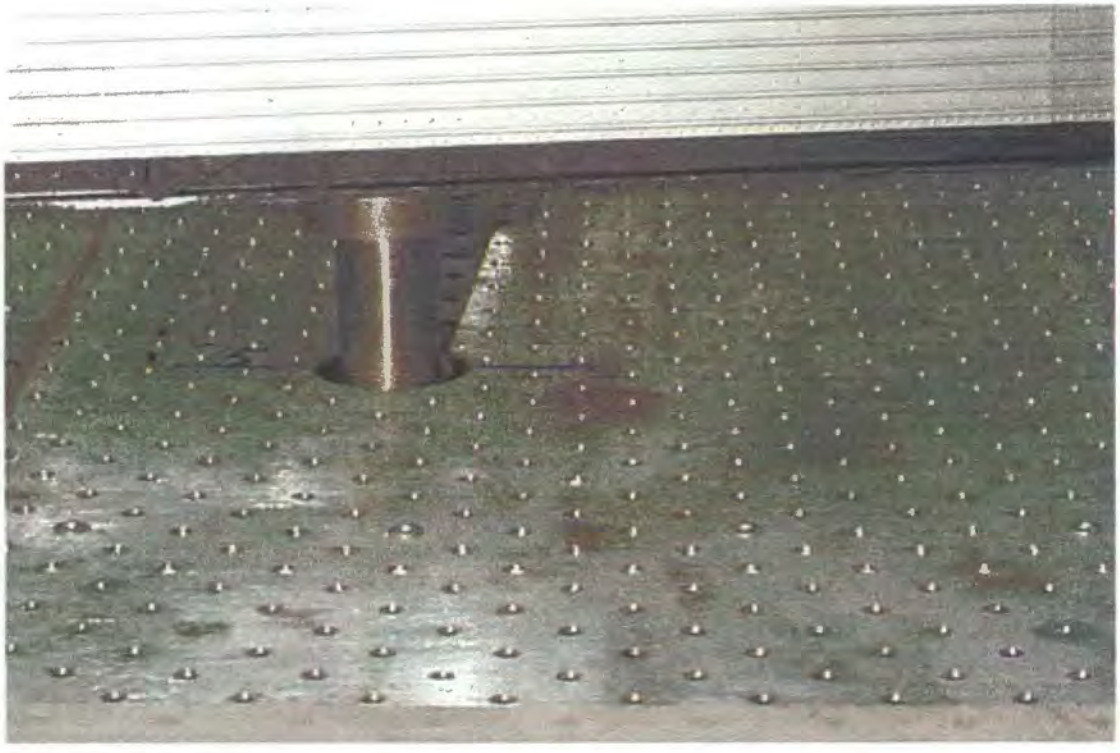

THE INFLUENCE OF GROUND CLEARANCE ON AERODYNAMIC DRAG

The first investigation into the effect that the boundary layer has on aerodynamic drag deals with the influence of ground clearance on aerodynamic drag.

It is a well understood fact that as an object is moved away from a surface, it gradually moves out of the boundary layer attached to that surface. In this case, as the truck is moved vertically away from the suction surface, it will gradually move out of the boundary layer attached to this suction surface. As it is moved out of the boundary layer, the average velocity of the air striking the truck at a certain place increases. From the momentum equation, this directly translates into a higher drag force. Also, due to more air moving below the truck, the friction on the under-body will also increase.

The truck was set at a minimum ground clearance of 5mm. This ground clearance was measured at the front axle. To ensure that the model was parallel to the suction floor, a spirit level was placed on the roof of the trailer. The ground clearance at the rear axle was also measured to ensure that the model was parallel to the ground. The reason for these numerous checks is that introduction of a wedge flow, i.e. or converging or diverging flow, below the truck would lead to adverse pressure gradients which affect the growth of the boundary layer below the truck. Every time the ground clearance was changed, the longitudinal alignment of the truck was checked to ensure that the yaw angle did not vary from one setting to the next. Introducing even small variations to the yaw angle would result in differing frontal areas and thus larger drag forces. All these tests in this section were conducted at zero degrees yaw angle.

The following graphs are a graphic representation of the results. Type 1 through 4 refer to various test simulations, with no skirting present on the model.

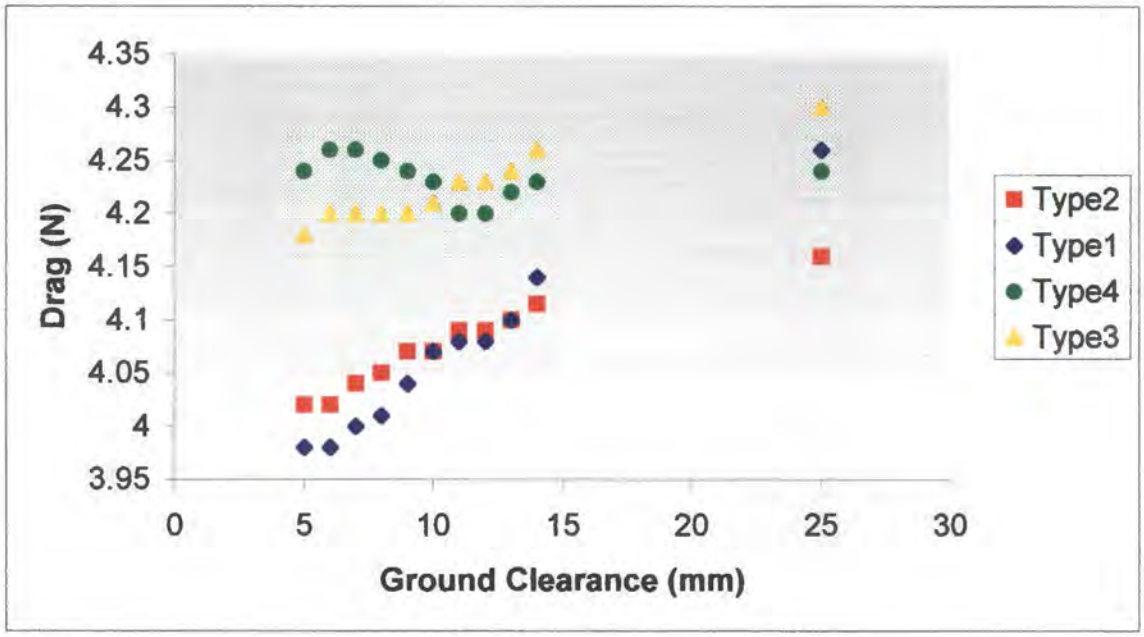

Fig. 4.1: Drag Readings for various simulation Types versus Ground Clearance.

The above graph reveals some very interesting points. The basic simulation, i.e. no suction and no rotation (Type2) shows that the expected trend is followed. This trend is that as the ground clearance is increased, the drag increases due to air striking certain vehicles parts at a higher velocity and a higher mass flux below the model. This trend is also followed by the simulation that is characterised by wheel rotation only (Type1) and wheel rotation and suction (Type3).

However, the Type4 simulation with only the suction on reveals an unexpected trend. Here the boundary layer is not present and the usually present pressure fields of the rotating wheels cannot influence the drag either. The aerodynamic drag peaks at a ground clearance of about 7mm. This simulation shows how important it is to simulate on road conditions as accurately as possible and also that the influence of the rotating wheels should not be neglected.

Of interest is the fact that the graphs representing Type 2 and Type 3 simulations are parallel and follow the same trend.

The question arises now which ground clearance should be chosen to continue with the testing. The drag is increasing as the ground clearance increases until the model is finally so far off the ground, that that no boundary layer can affect it.
To this end, the relative drag change for each ground clearance was computed for the Type3 simulation. The relative drag change is defined as

$$\Delta F_D = 100\left(1 - \frac{F_D'}{F_D}\right) \qquad 4.1$$

Here F_D' indicates the drag reading for the Type2 simulation.
The following graph is thus obtained.

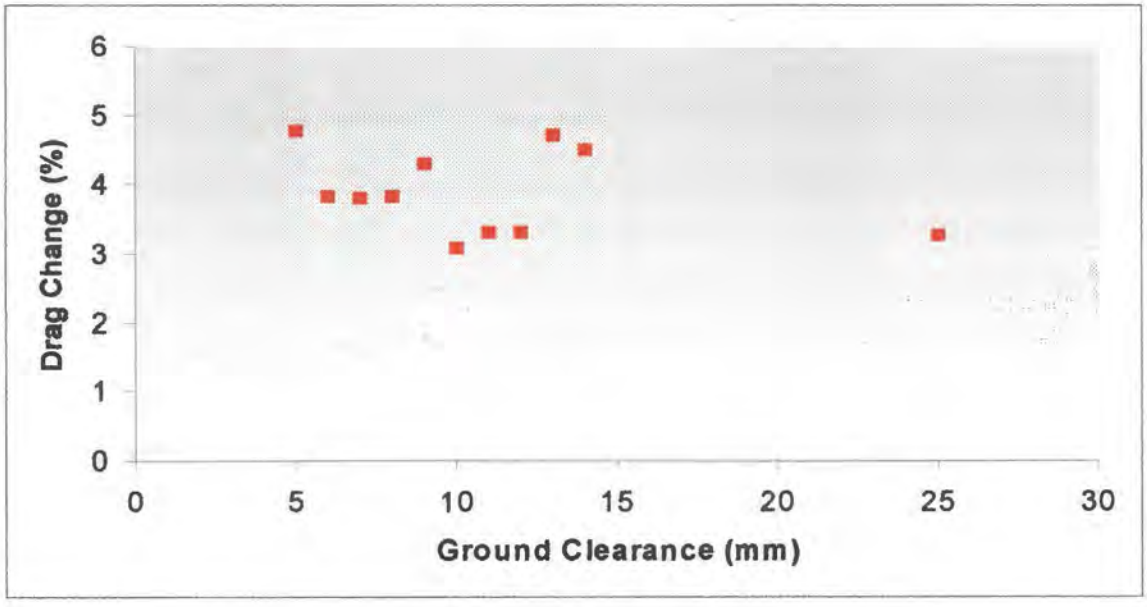

Fig. 4.2: Drag change for Type3 Simulation versus Ground Clearance.

The graph does not provide any conclusive evidence about the height at which the most drastic change in drag occurs. The values calculated seem random and do not indicate any fixed pattern. However, looking at the absolute values of the drag changes indicates that these changes lie within the three to five percent bracket. These changes are slightly higher than European tests revealed. This variance can be put down to the fact that up to 89% of the boundary layer displacement thickness was removed, compared to only 67% for the European Wind Tunnel at Porsche[22].

It was thus decided to keep the ground clearance as small as possible without jeopardising the drag reading. The only way that the drag reading could be jeopardised is through model contact with the suction surface. Also, due to the high rotational speeds involved, the tyres tend to increase in diameter, sometimes up to 3 to 4mm. The above considerations prompted the author to mount the model 6mm above the ground. Again, the six millimeters is measured at the front axle and means that when the wheels are not rotating, the clearance between the outer rubber and the ground is 6mm.

DRAG COEFFICIENT AT VARIOUS REYNOLDS NUMBERS

A basic requirement for correct wind tunnel testing calls for dynamic similarity between the on road conditions and the test conditions. This requires that the Reynolds numbers in both cases must be the same. However, if a 1/24 scale model is tested, the above requirement would result in the speed in the wind tunnel being 24 times the on-road speed. This high speed would introduce compressibility effects and is thus not viable.

SAE tests [SAE J1252] have shown that the Reynolds number should not fall below 700.000. Some researchers have even suggested Reynolds Numbers not below 1.300.000.
This would however not be possible with a 1/24 scale model in the low speed wind tunnel. Also, the type of research being undertaken calls for the Reynolds number to be based on the square root of the frontal area.

It was decided to examine the effect that the various speeds in the low speed wind tunnel would have on the Reynolds number, Fig. 3.3.

This test showed that the drag coefficient remains fairly constant from about a Reynolds Number of 100.000 based on the square root of the frontal area onwards. The above tests were done with the skirting present on the model.

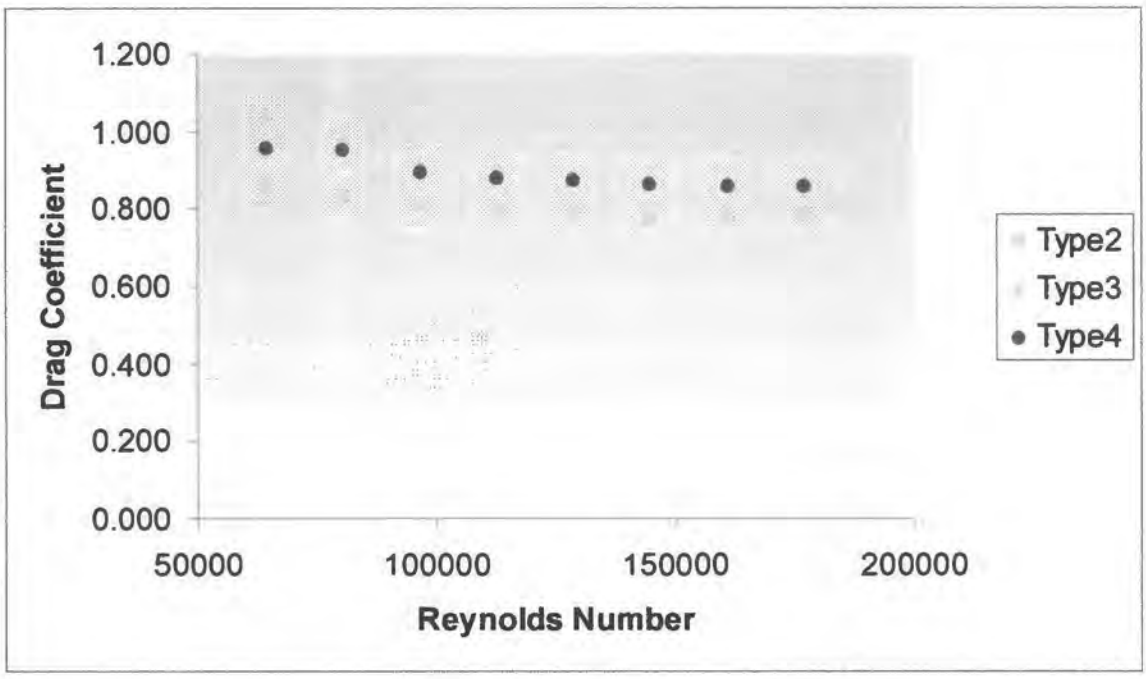

Fig. 4.3: Drag Coefficient versus Reynolds Number.

DRAG COEFFICIENT AND YAW ANGLE

The model was now subjected to air striking it at an angle. To accurately reflect the results, all measured forces and velocities were converted to a body axis system referred to the model.

The drag that is measured by the balance is the drag that the sting support experiences. This drag is thus reflected as a body axis drag on the three component balance. To convert this reading to the body axis system of the model, the components in the body axis system of the model must be determined.

Graphically, the solution is found as follows:

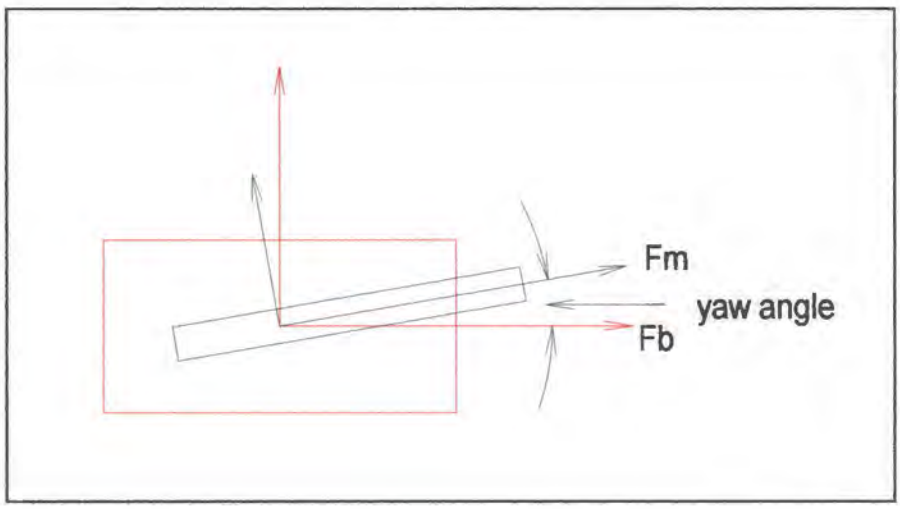

Fig. 4.4: Body Axis and Balance Axis System with Yaw Angle.

Here the angle between the force as measured by the balance (Fb) and the force in the body axis component (Fm) is the yaw angle. Thus,

$$F_M = F_b \cos\psi \qquad 4.2$$

The same calculation applies to the oncoming air.

The above considerations allow the reference frontal area of the truck to remain the same, even at yaw conditions. The alternative to this would be to determine the projected frontal area at yaw. This approach in turn would not require the component calculations of the force and velocity. Taking mathematical considerations into account it is easier to work with a body axis system of the model and not with a body axis system of the balance or wind tunnel. The wind tunnel and balance share the same body axis system, because both are perfectly aligned in all three axes.

The solutions presented on the following pages compare the model without skirts to the model with skirts at the same non-rotating wheel clearance of 6mm. The skirts effectively lower the overall vehicle clearance by 20mm, leaving a 8mm ground clearance.

The yaw angles were changed at 4 degree increments and were marked on the surface of the suction box. At higher yaw angles the truck started to rotate due to the high forces acting on the trailer. This problem was however quickly overcome by using a tapered bolt to hold the sting in the component balance. Also, the bolt was tightened more than in the previous tests. After each change of the yaw angle, a spirit level was used to ensure that the model remained level. Ground clearance was also checked.

Following is a photograph of the model at 16 degrees yaw taken from above.

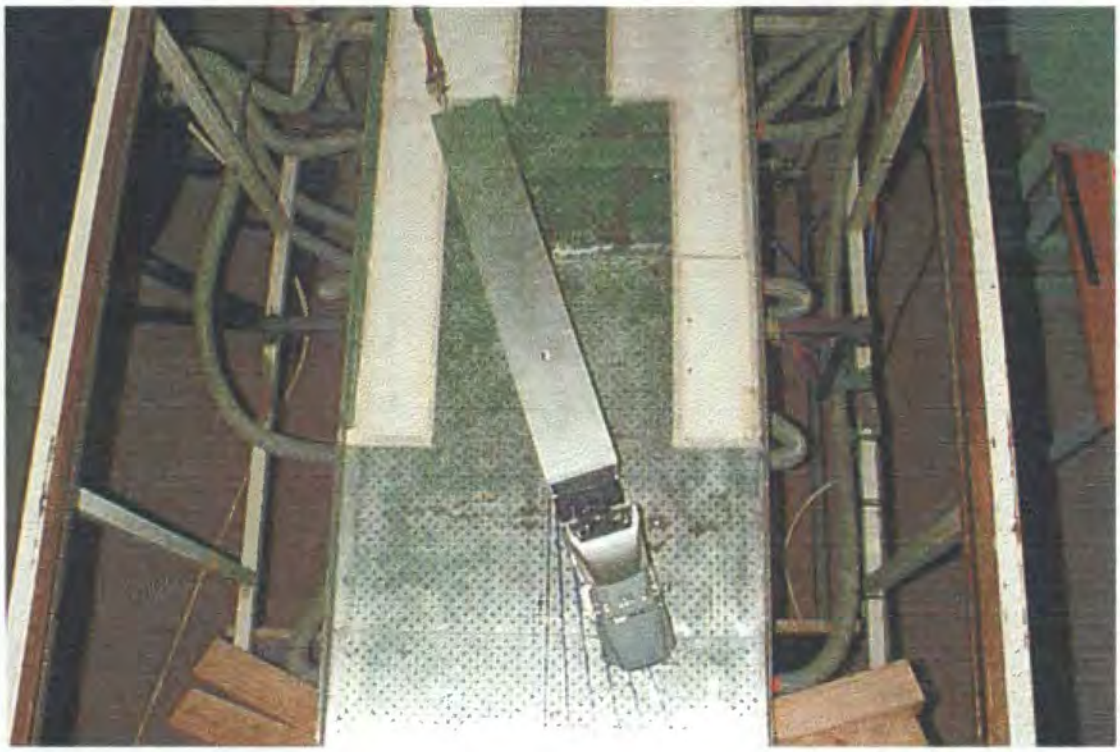

The following photograph is taken from the front and clearly shows the skirting and the high amount of model detail.

The following four graphs compare the aerodynamic forces acting on the model with and without skirts for Type1 to Type4 simulations

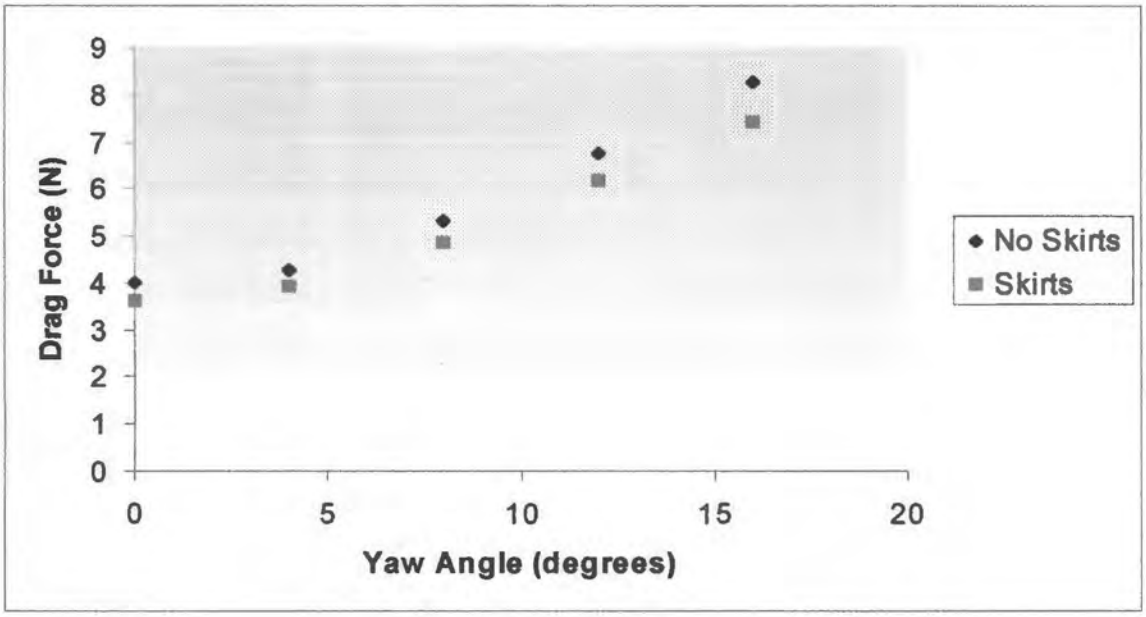

Fig. 4.5: Drag force for Type1 versus Yaw Angle.

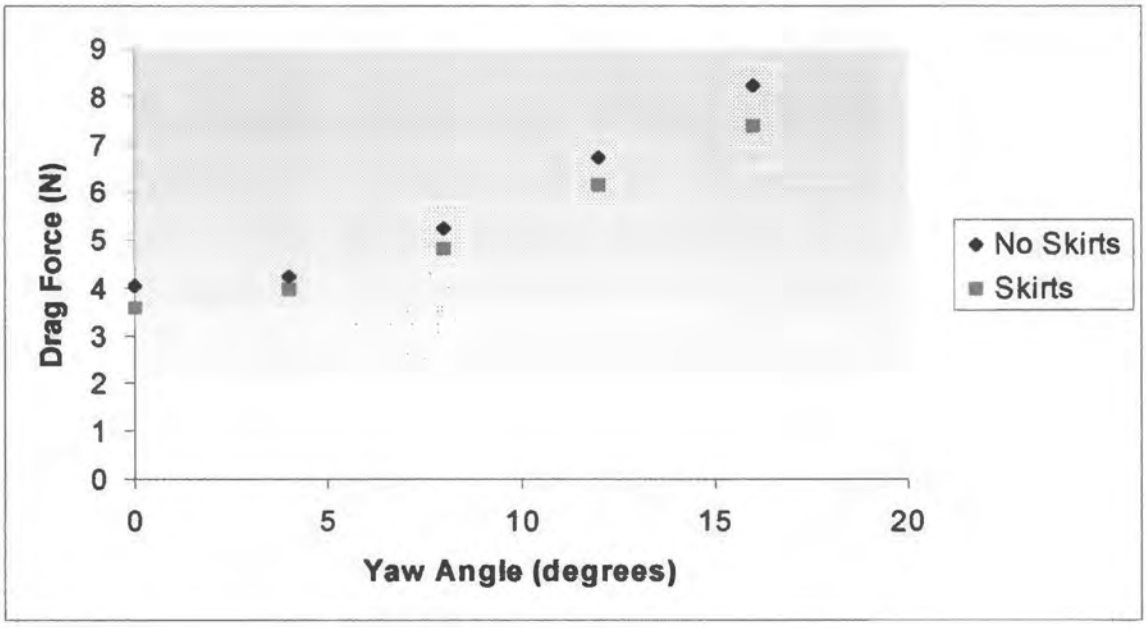

Fig. 4.6: Drag force for Type2 versus Yaw Angle.

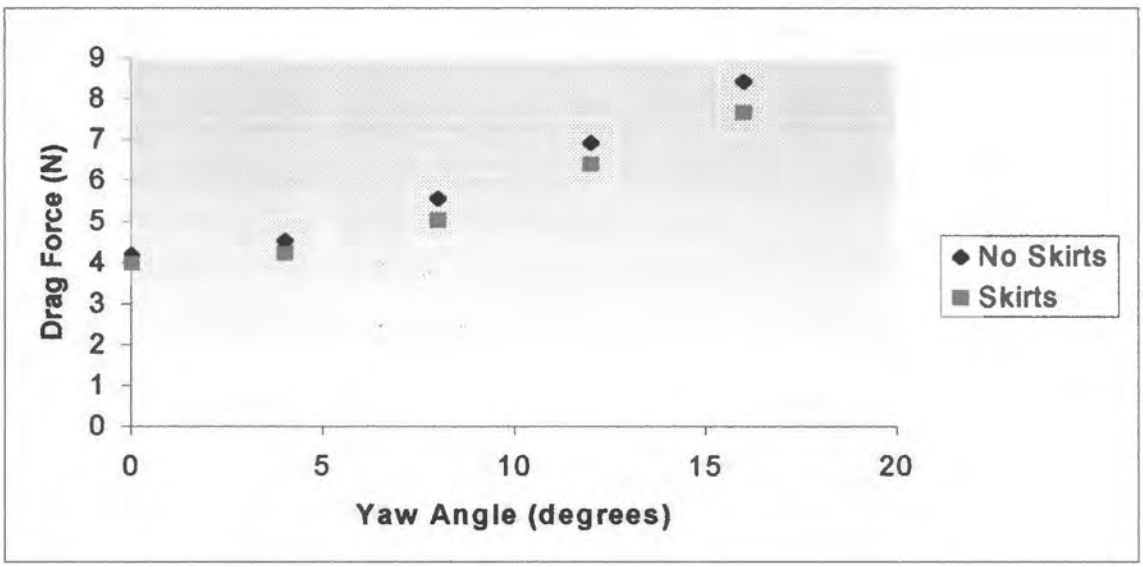

Fig. 4.7: Drag Force for Type3 versus Yaw Angle.

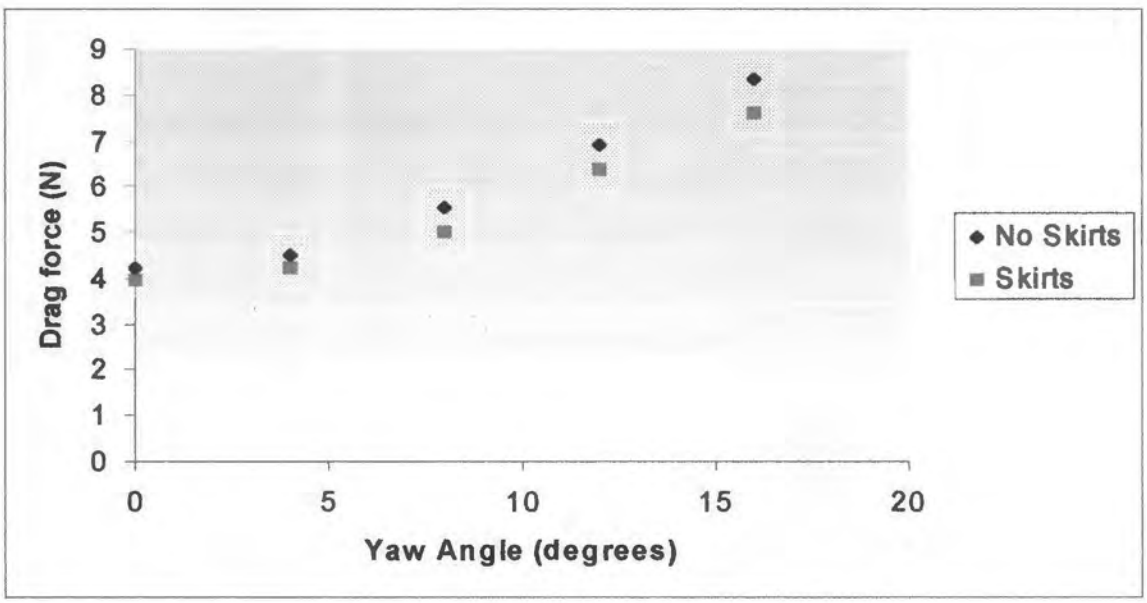

Fig. 4.8: Drag force for Type4 versus Yaw Angle.

All of the above simulations follow the same trend. The model fitted with the skirts shows a remarkably lower drag than the model without the skirts. This is due to the lower airflow below the truck and thus less drag forming due to the underbody of the model. This effect is amplified at higher yaw angles. The reason for this could possibly be the smaller size of the wake and therefore a reduced pressure drag in the case with the model with skirts. Less air flows beneath the truck and this reduces the size of the wake. Also, most of the underbody is shielded from the direct oncoming airflow.

The above results indicate the importance of shielding the underbody from the airflow as much as possible. However, physical limitations place a limit on the amount of skirting, as trucks frequently have to negotiate ramps and other obstacles on the roads.

The following graphs will examine the effect of the boundary layer on the drag by comparing the simulation types with the model featuring skirts and no skirts.

For clarity, the graphs show the drag coefficient, as opposed to the drag forces in the previous graphs.

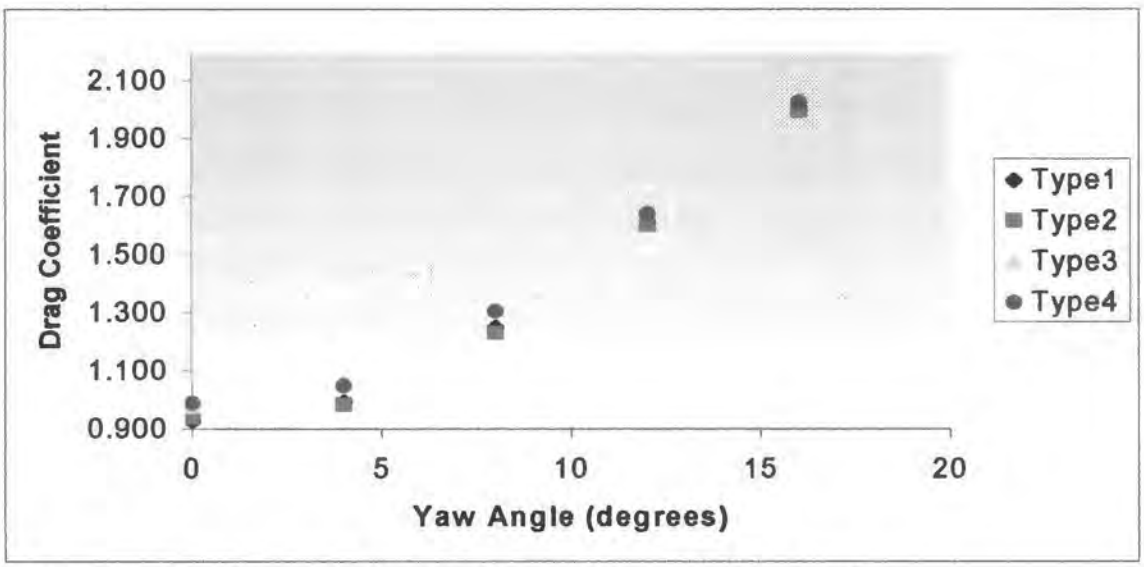

Fig. 4.9: Drag Coefficients for Model without Skirts versus Yaw Angle

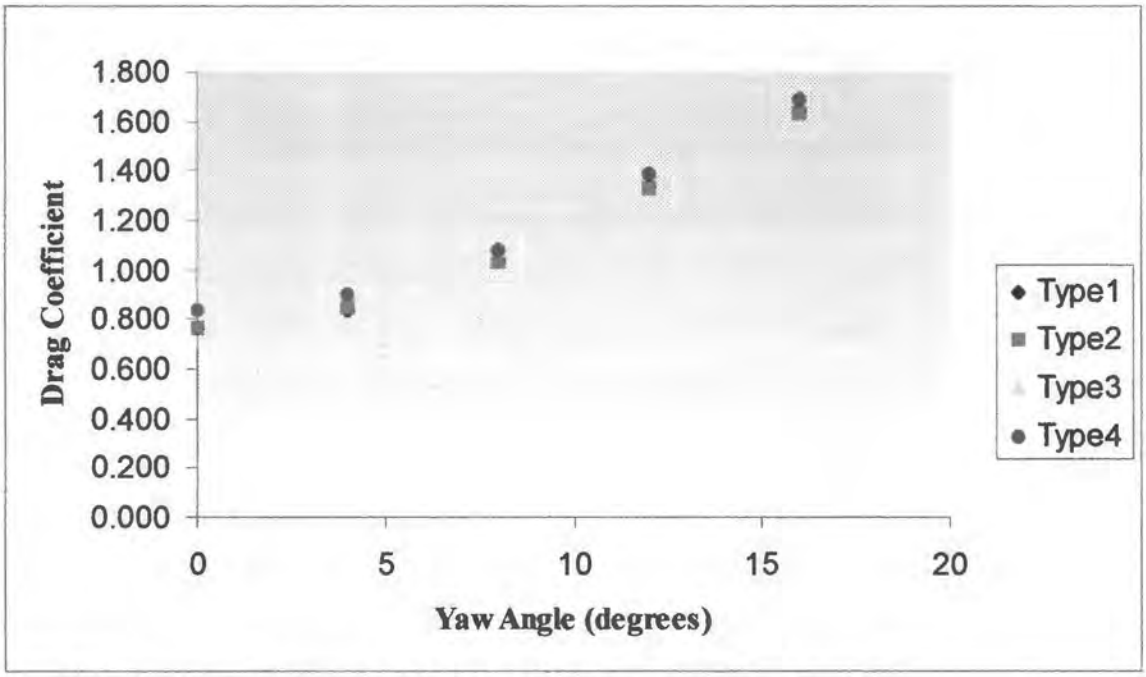

Fig. 4.10: Drag Coefficients for Model with Skirts versus Yaw Angle

Again both sets of the data follow the same trend, with increasing yaw angle the drag coefficient increasing accordingly. However, the coefficient values for the model without skirts are remarkably higher than the ones with skirt. The reason for this lies in the higher underbody drag force which the model without skirts experiences.

The differences in drag coefficient between the Type2 and Type3 simulations are shown below, both for the model with skirts and without skirts.

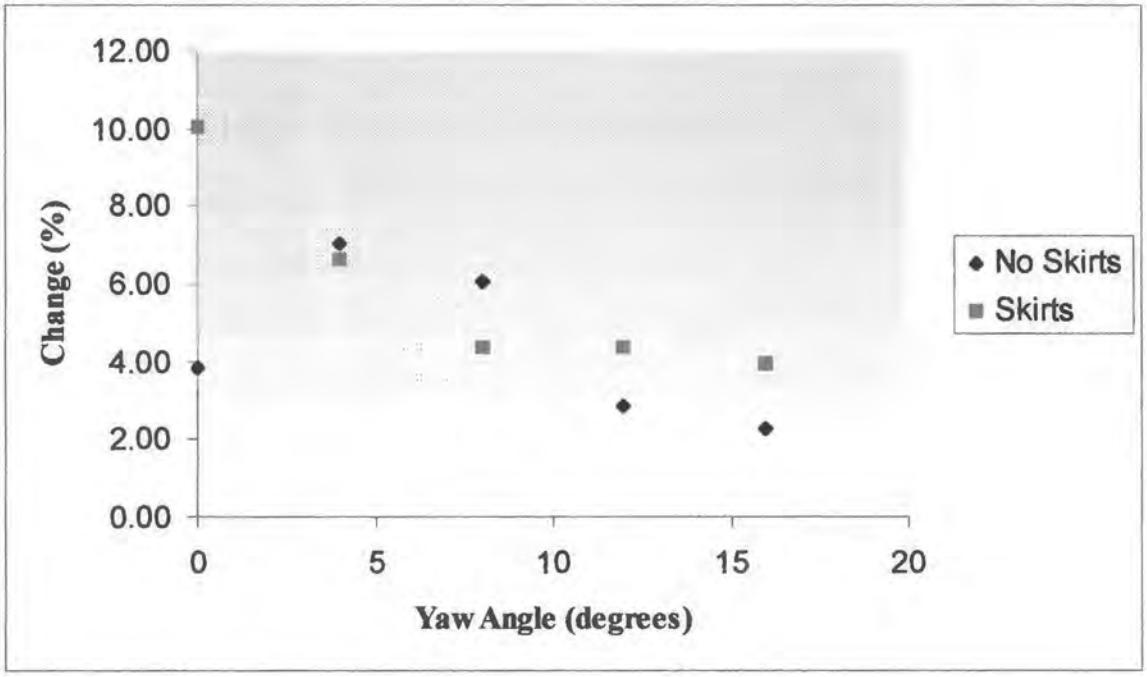

Fig. 4.11: Drag Coefficient Change versus Yaw Angle.

The model with skirts follows the trend that with increasing yaw angle, the difference in drag coefficient between Type 2 and Type 3 simulations decreases. A 10% change is seen at zero degrees yaw angle. This means that there is a considerable difference between the readings with the boundary layer present and without the boundary layer. The model without skirts first shows an increase in the change of the drag coefficient, but the change is seen to decrease again as the yaw angle increases.

A possible reason for this diminishing change is that as the model is yawed, the surface area that the air strikes directly increases rapidly. The influence of the boundary layer decreases because the increase in drag force due to the larger area is by far greater than the increase in drag due to removal of the boundary layer.

CHAPTER 5 - CONCLUSIONS

Based on the research undertaken, the following conclusions can be drawn:

The removal of the boundary layer was accomplished satisfactorily. The aim of the boundary layer removal approach is that the boundary layer at the beginning of the model must be as thin as possible. The approaching boundary layer was reduced from 15.75mm to 8.75mm, a reduction of 56%, measured at the front of the model. The boundary layer displacement thickness was reduced from 2.67mm to 0.3mm. This is a massive reduction of 89%. These figures refer to an ambient wind speed of 22.2 m/s.
A comparison to the effectiveness of this system compared to other boundary layer removal devices can now be drawn. The data which was most readily available for this purpose refers to the Porsche Wind Tunnel. The device employed to remove the boundary layer by means of suction achieved a decrease from 12mm to 6mm at the front of the model, a reduction of 50%. These figures refer to an ambient wind speed of 57 m/s.

The model of the truck was tested with and without skirts. The skirts lowered the ground clearance by 25mm. The Suction Off, Rotation Off is the zero simulation condition, where no simulation was applied. This condition was thus taken as the reference point. All data is referred to this point. With the suction off and rotation of the wheels on (Type1), drag was reduced by 1% for the model without skirts and the drag increased by about .05% for the model with skirts. For Type4 simulation, i.e. suction on and rotation of the wheels off, an increase of 5.2% for the model without skirts and 9.1% for the model with skirts was achieved. Type3 simulation, i.e. rotation and suction on, resulted in a aerodynamic drag increase of 3.8% for the model

without skirts and 10% for the model with skirts.
A similar study into the effect of the boundary layer showed that the aerodynamic drag could increase from between 1.3% to 3.7% without the presence of the boundary layer.

The above results refer to zero degrees yaw and a free stream velocity of 22.2m/s or 80km/h. The same behaviour was observed at different yaw angles. As can be seen, due to the higher flow rate of air below the model, the drag is increased when the ground boundary layer is removed. The influence of wheel rotation was also examined. The reason for the higher values for the model with skirts is that the model penetrates far deeper into the boundary layer, and thus the effect of removing this boundary layer is greater than with the other models. The fitting of the skirts to the model resulted in a reduction of 9% for the drag.
With this type of ground simulation it is thus possible to effectively remove the oncoming boundary layer. This will then allow the design team to accurately test vehicles in a wind tunnel without the disturbing boundary layer present.

CHAPTER 6 - RECOMMENDATIONS

The investigation presented showed that the boundary layer could be removed effectively. However, certain improvements could be undertaken to further fine tune the results.

It would be very interesting to examine the influence of the model on the boundary layer in front of the model and below the model. Very fine and small pitot tubes would have to be used for this investigation.

This understanding of the behaviour of the boundary layer with the model present can then be used to define and improve the suction system for the boundary layer removal system even further. For example, certain suction rates could be applied to different surfaces by introducing smaller suction compartments within the larger suction box. Each suction compartment would then feature its own dedicated fan to remove the boundary layer over this patch of the suction surface. Calibration would then be done with the model present.

This device could then be used to understand the complicated flow patterns of ground vehicles where the ground clearance is of critical importance. Given a balance which can be connected to the model via a rear sting, detailed studies of lift, drag and moments could then be undertaken without the sting holding the model from below and thus influencing the flow patterns.

CHAPTER 7 - REFERENCES

1. Garry, K.P., "*A Review of Commercial Vehicle Aerodynamic Drag Reduction Techniques.*" IMECH 1985, 1985.
2. Ohlson, M.E., Schaub, U.W., "*Aerodynamics of Trucks in Wind tunnels: The Importance of Replicating Model Form and Detail, Cooling system and Test Conditions.*" SAE 920345, 1992.
3. Saunders, J.W., Watkins, S., Hoffmann, P.H., Buckley, F.T., "*Comparison of On – Road and Wind Tunnel Tests for Tractor – Trailer Aerodynamic Devices, and Fuel Saving Predictions.*" SAE 850286, 1985
4. Cooper, K.R., Mason, W.T., Bettes, W.H., "*Correlation Experience With SAE Wind tunnel Test Procedure for Trucks and Buses*". SAE 820375, 1982
5. Modi, V.J., Hill, S.St., Yokomizo, T., "*Drag Reduction for Trucks Through Boundary Layer Control*". Journal of Wind Engineering and Industrial Aerodynamics 54/55, 1995
6. Mercker, E., Knappe, H.W., "*Ground Simulation with moving Belt and Tangential blowing for Full Scale Automotive Testing in a Wind Tunnel*". SAE890367, 1989
7. Drollinger, R.A., "*Heavy Duty Truck Aerodynamics*". SAE87001, 1987
8. Kuenstner, R., Deutenbach, K.R., Vagt, J.D., "*Measurement of Reference Dynamic Pressure in Open Jet Automotive Wind Tunnels*". SAE920344, 1992
9. Sardou, M., "*Moving Ground and Reynolds number Effect on Tractor Trailer*". SAE 870707, 1987
10. Beauvais, F.N., Tignor, S.C., Turner, T.R., "*Problems of Ground Simulation in Automotive Aerodynamics*". SAE 680121, 1968
11. Waudby-Smith, Rainbird, W.J., "*Some Principles of Automotive Aerodynamic Testing in Wind Tunnels with Examples from Slotted Wall Test Section Facilities*". SAE850284, 1985

12. Bearman, P.W., De Beer, D., Hamidy, E., Harvey, J.K., "*The Effect of a Moving Floor on Wind Tunnel Simulation of Road Vehicles*". SAE880245, 1988
13. Cooper, K.R., " *The Effect of Front Edge Rounding and Rear Edge Shaping on the Aerodynamic Drag of Bluff Bodies in Ground Proximity*". SAE850288, 1988
14. Berndtsson, A., Eckert, W.T., Mercker, E. " *The Effect of Ground Plane Boundary Layer Control on Automotive Testing in a Wind Tunnel*". SAE880248, 1988
15. Kettinger, J.N., "*Tractor Trailer Fuel Savings with an Aerodynamic Device , A Comparison of Wind Tunnel and On Road Tests*". SAE820376, 1982
16. Watkins, S., Saunders, J., "*Wind Tunnel Modelling of Commercial Vehicle Drag Reduction Devices*". SAE870717, 1987
17. Burgin, K. Adey, P.C., Beatham, J.P., " *Wind Tunnel Test on Road Vehicle models using a moving Belt Simulation of Ground Effect*". Journal of Wind Engineering and Industrial Aerodynamics 22, p227-236,1986
18. Garry, K.P., "Some Effects of Ground Clearance and Ground Plane Boundary Layer Thickness on the Mean Base Pressure of a Bluff Vehicle Type Body". Journal of Wind Engineering and Industrial Aerodynamics 62, p1-10, 1996
19. Ahmadi, M., Garry, K.P., "Preliminary Investigation of the Influence of a Ground Plane Boundary Layer on the Aerodynamic Characteristics of Road Vehicle Models Tested over a Fixed Ground". SAE 960675, 1996
20. Wiedemann, J., "*Some Basic Investigations into the Principles of Ground Simulation Techniques in Automotive Wind Tunnels*". SAE890369, 1989
21. Wiedemann, J., "*The Influence of Ground Simulation and Wheel Rotation on Aerodynamic Drag Optimisation, Potential for Fuel Consumption*". SAE960672, 1996
22. Vagt, J.D., Wolff, B., "*Das Neue Meßzentrum für Aerodynamik, Zwei Neue Windkanäle bei Porsche, Teil 1&2*". ATZ, 1987
23. SAE Recommended Practice, "*Wind Tunnel Test Procedures for Trucks and Buses*". SAEJ1252, 1968

24. Holman, J.P., "*Experimental Methods for Engineers.*" McGraw Hill 5th Edition, 1989
25. Chapra, S., "*Numerical Methods for Engineers*". McGraw hill 2nd Edition, 1990
26. Sayers, A.T., "*Fluid Mechanics, an Introduction*". Oxford 1992

APPENDIX A

This appendix contains all the drawings that were drawn up for the ground simulation using a belt as moving ground.

- Figure A-1
- Figure A-2
- Figure A-3
- Figure A-4
- Figure A-5
- Figure A-6
- Figure A-7
- Figure A-8
- Figure A-9
- Figure A-10
- Figure A-11
- Figure A-12

FIGURE A-1

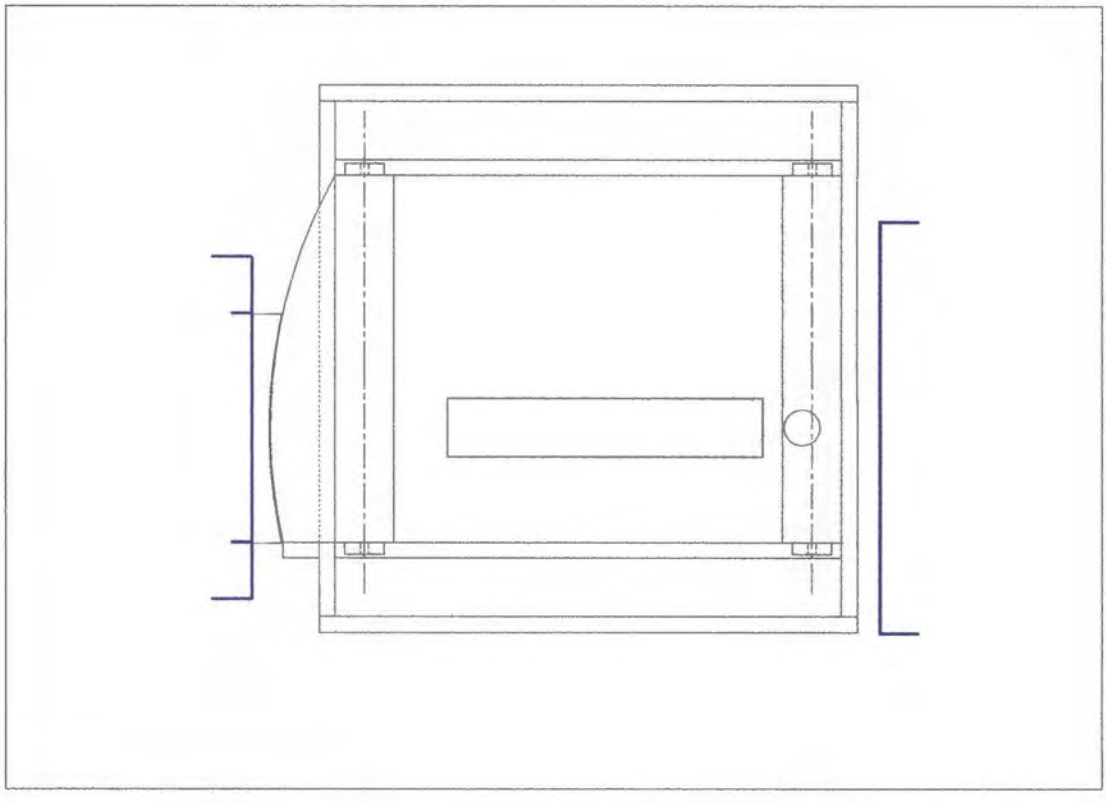

FIGURE A-2

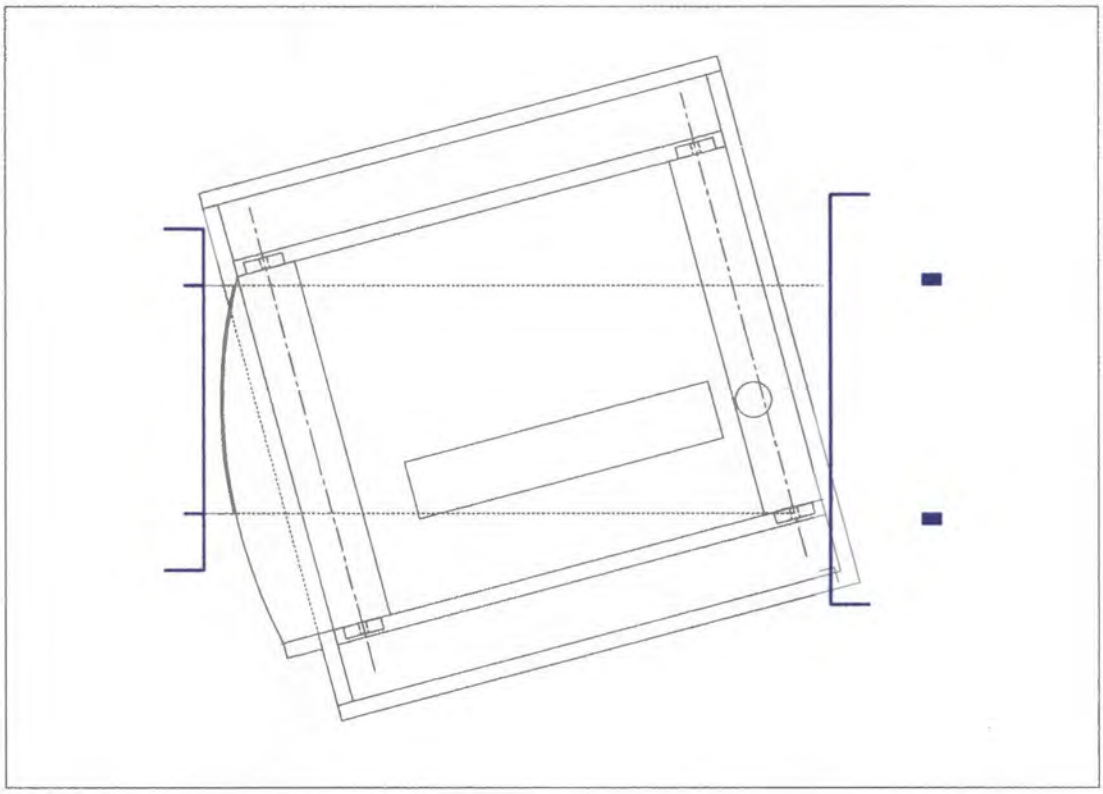

FIGURE A-3

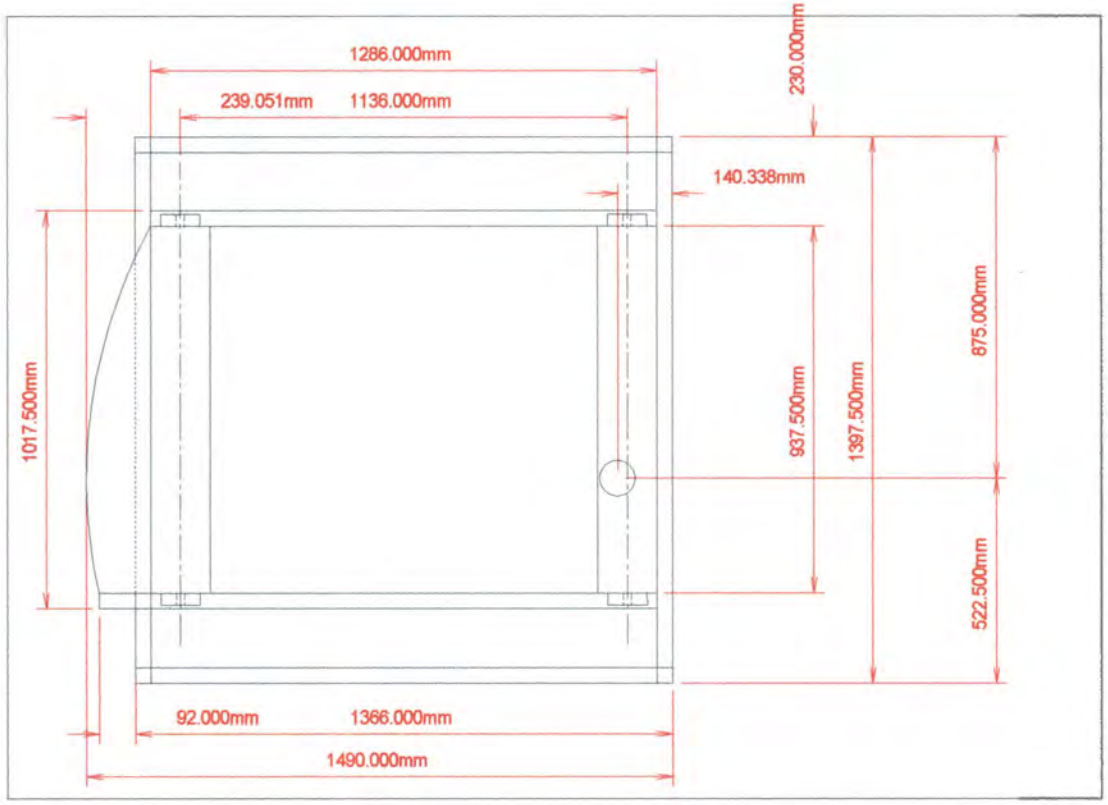
1286.000mm
239.051mm
1136.000mm
230.000mm
140.338mm
1017.500mm
937.500mm
1397.500mm
875.000mm
522.500mm
92.000mm
1366.000mm
1490.000mm

FIGURE A-4

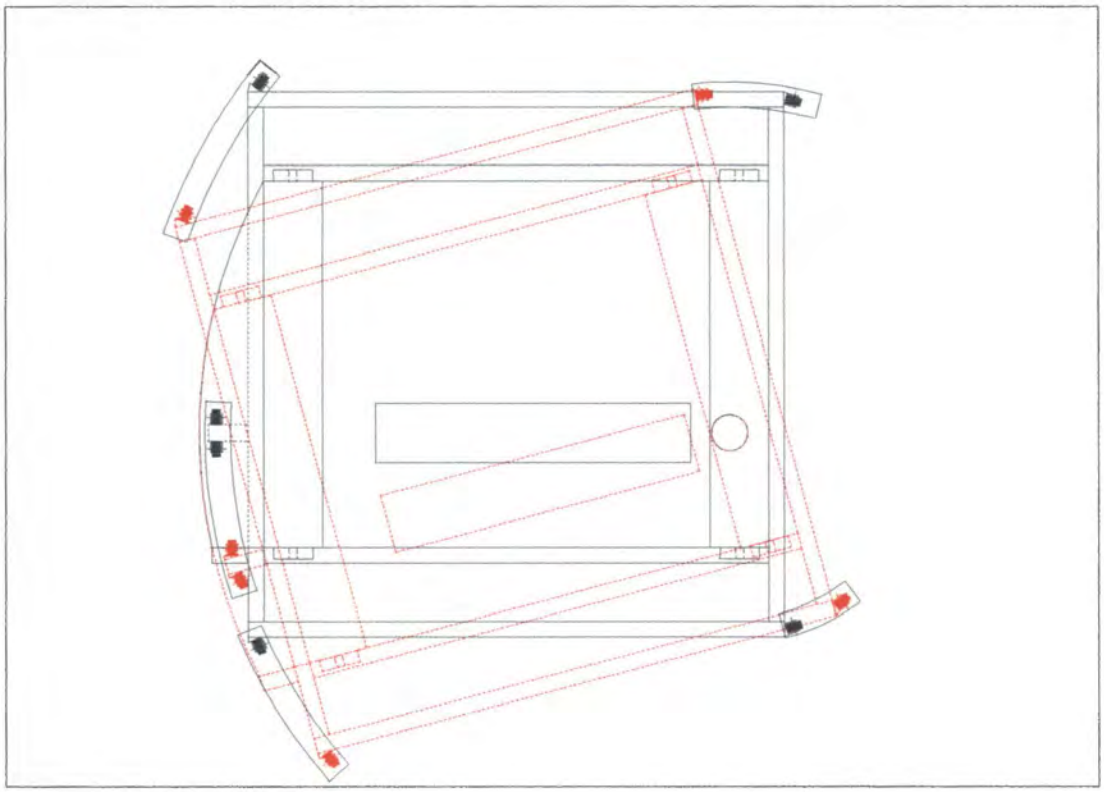

FIGURE A-5

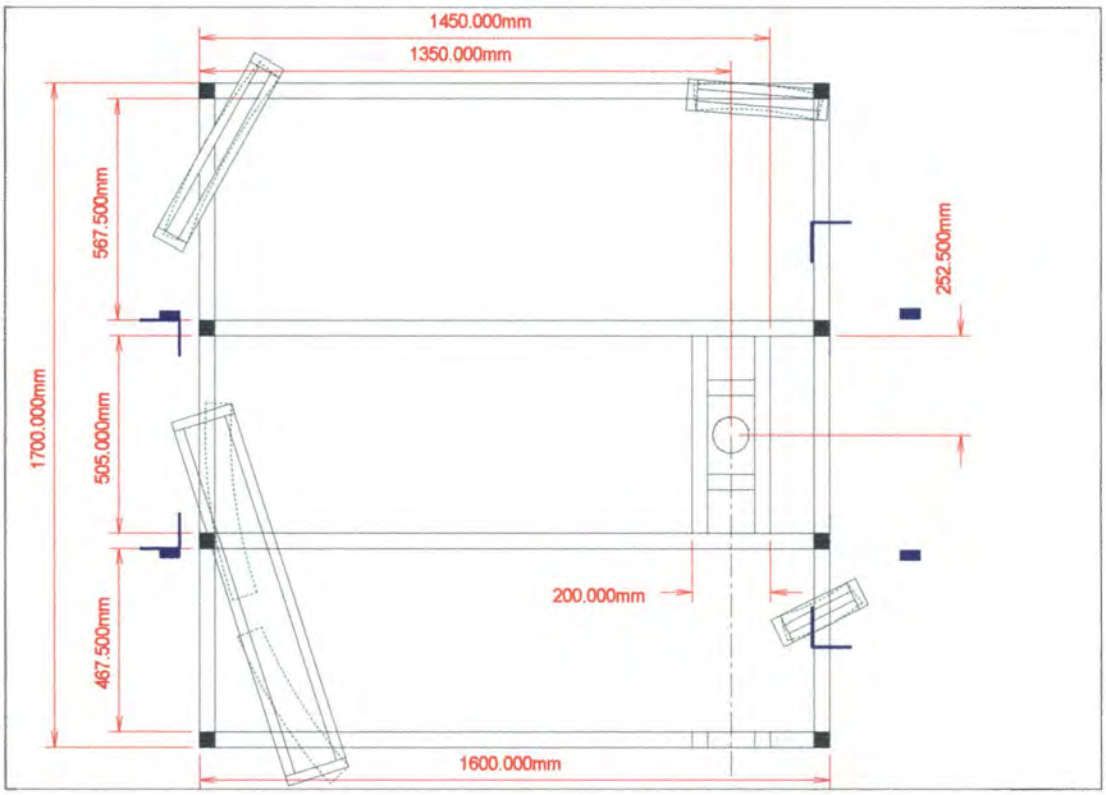
1450.000mm
1350.000mm
567.500mm
252.500mm
1700.000mm
505.000mm
200.000mm
467.500mm
1600.000mm

FIGURE A-6

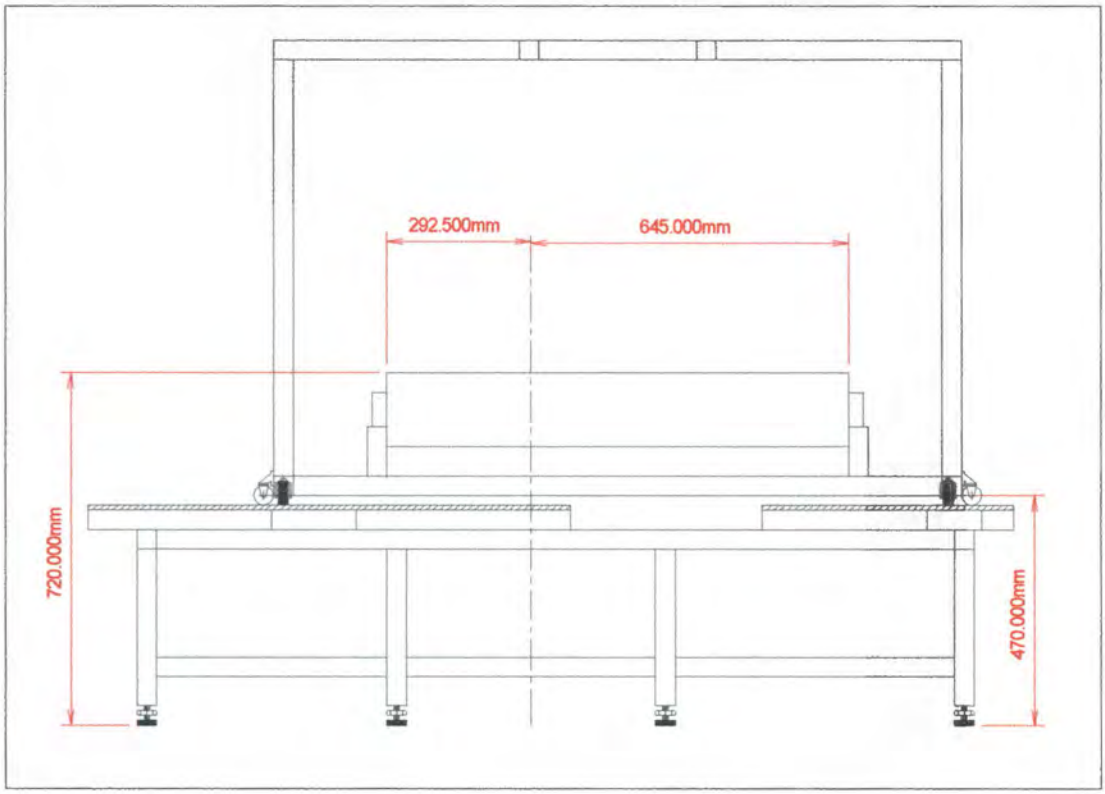

FIGURE A-7

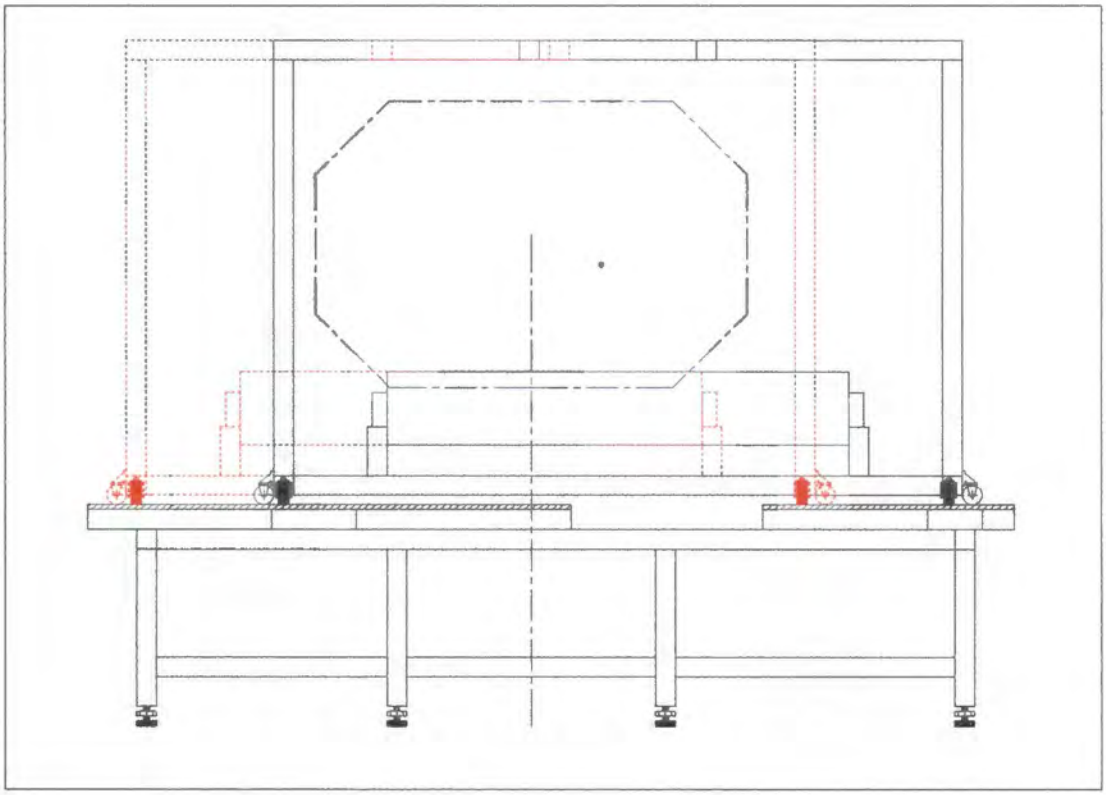

FIGURE A-8

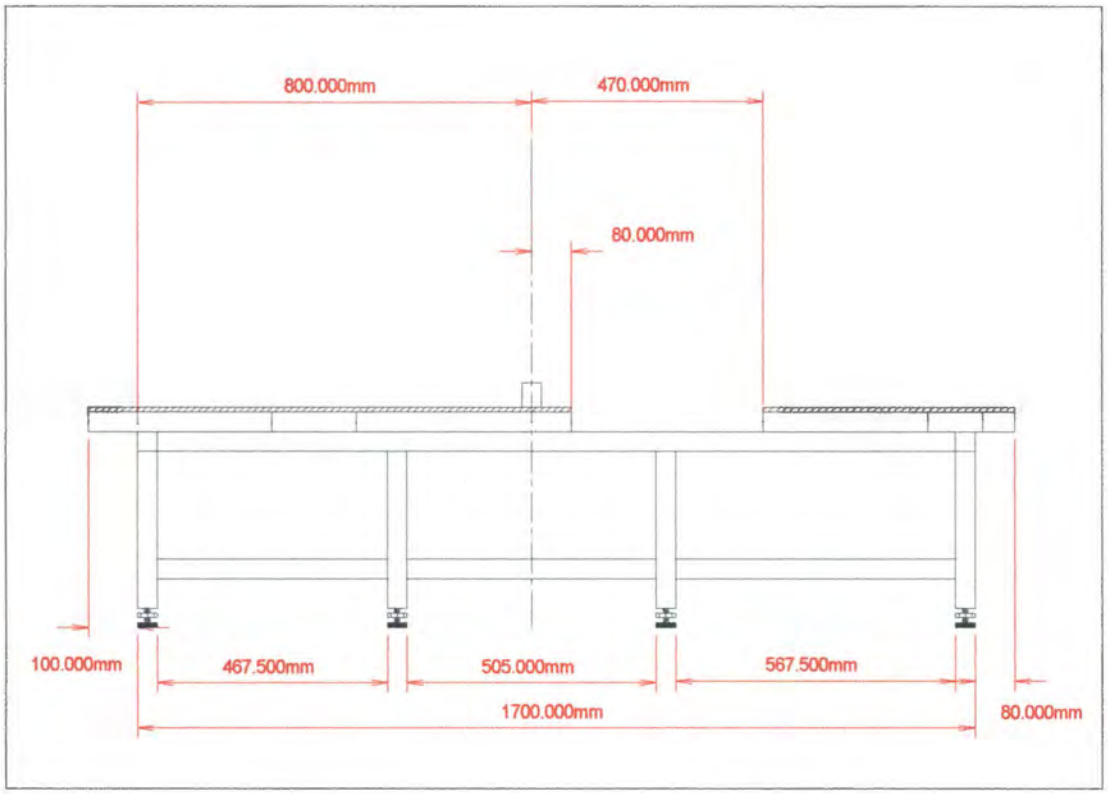
800.000mm
470.000mm
80.000mm
100.000mm
467.500mm
505.000mm
567.500mm
1700.000mm
80.000mm

FIGURE A-9

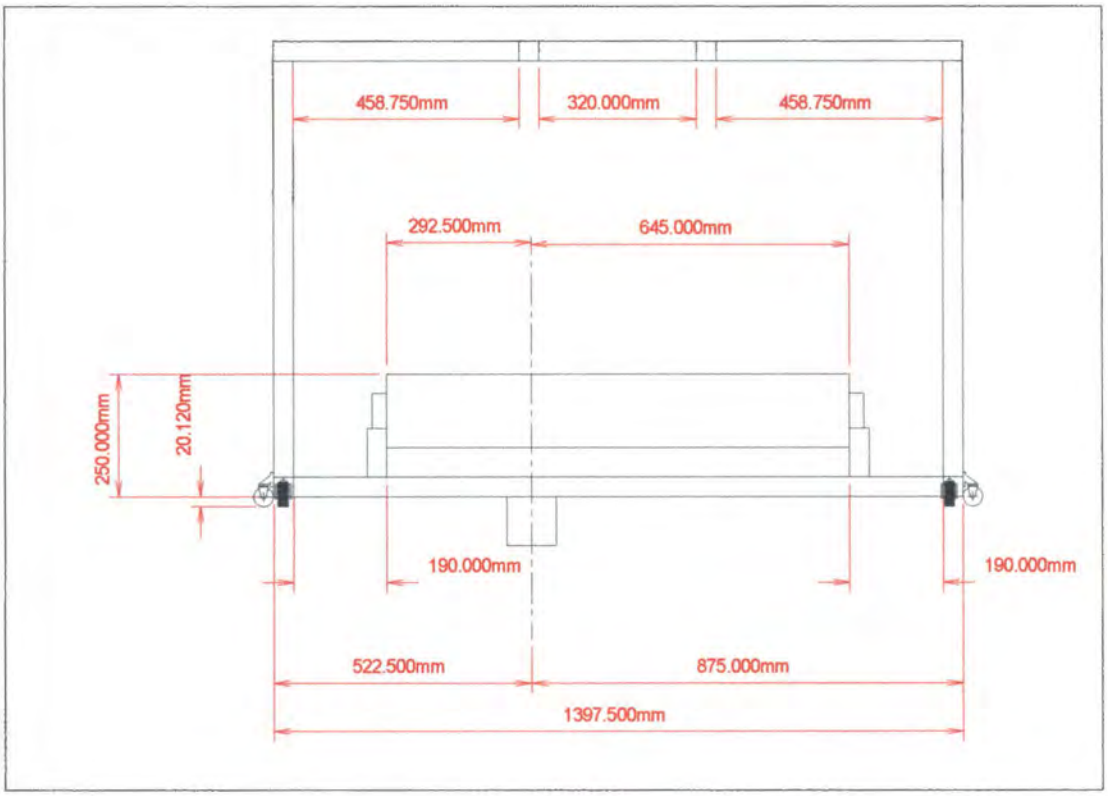
458.750mm
320.000mm
458.750mm
292.500mm
645.000mm
250.000mm
20.120mm
190.000mm
190.000mm
522.500mm
875.000mm
1397.500mm

FIGURE A-10

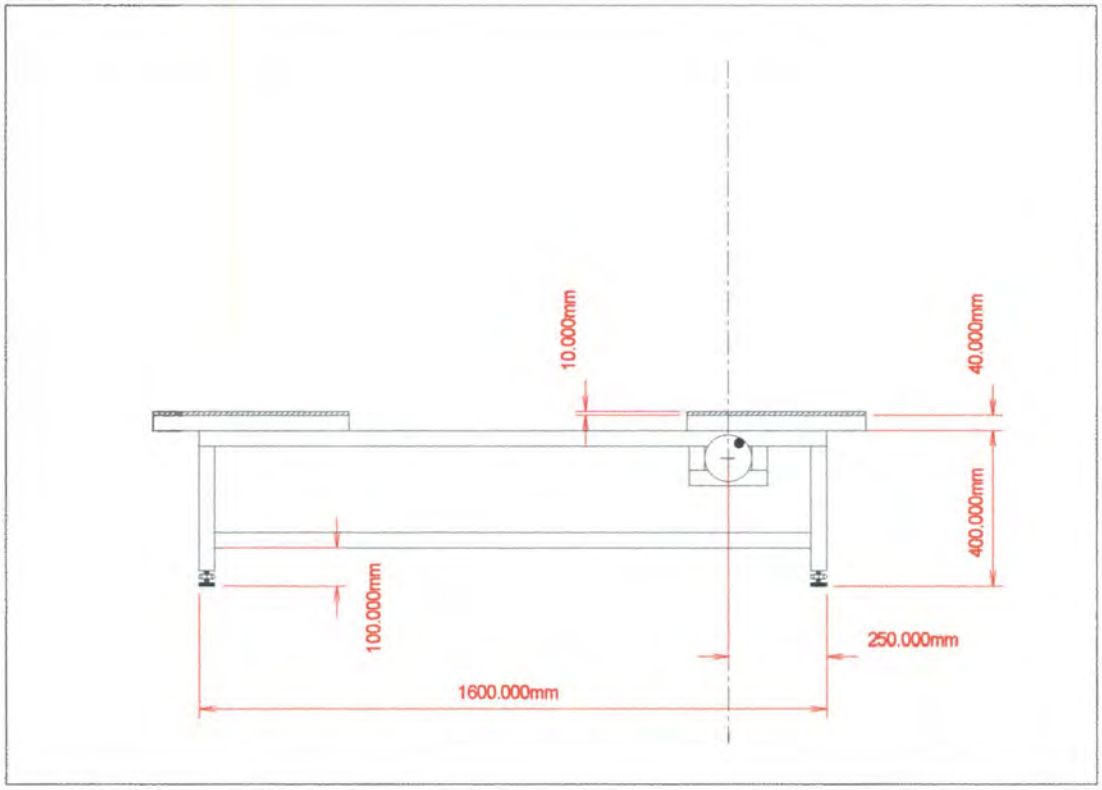

FIGURE A-11

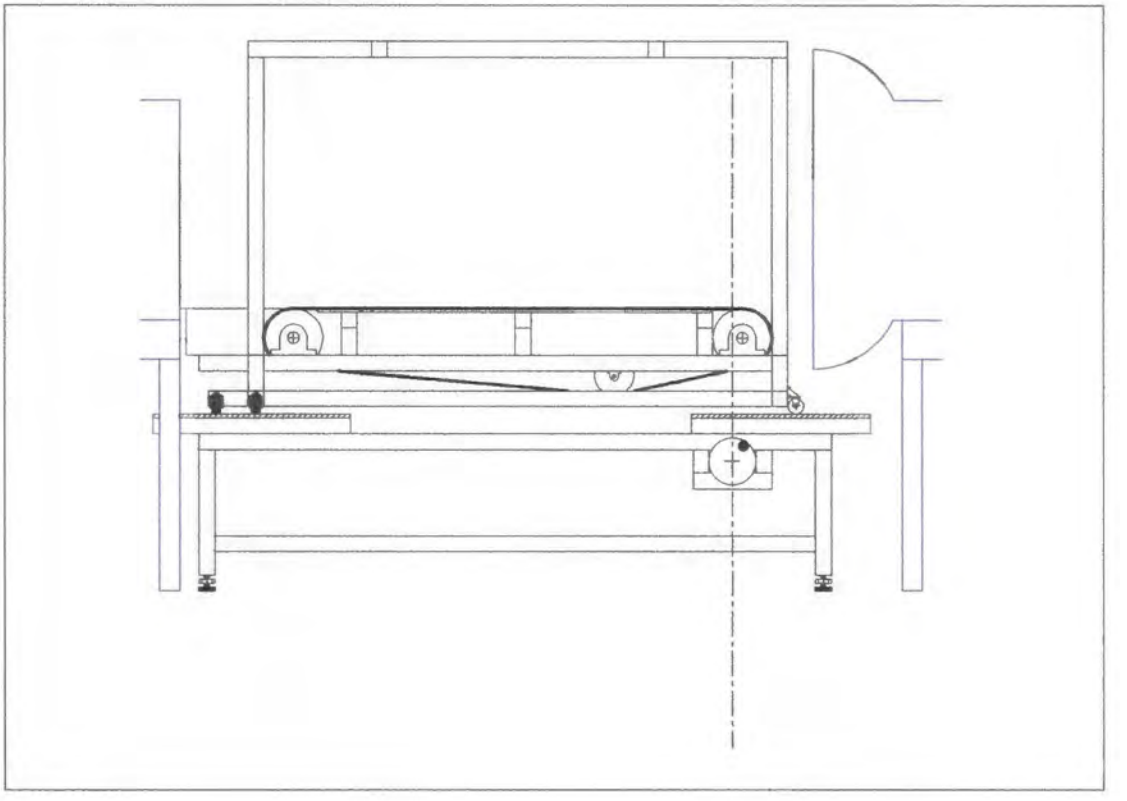

FIGURE A-12

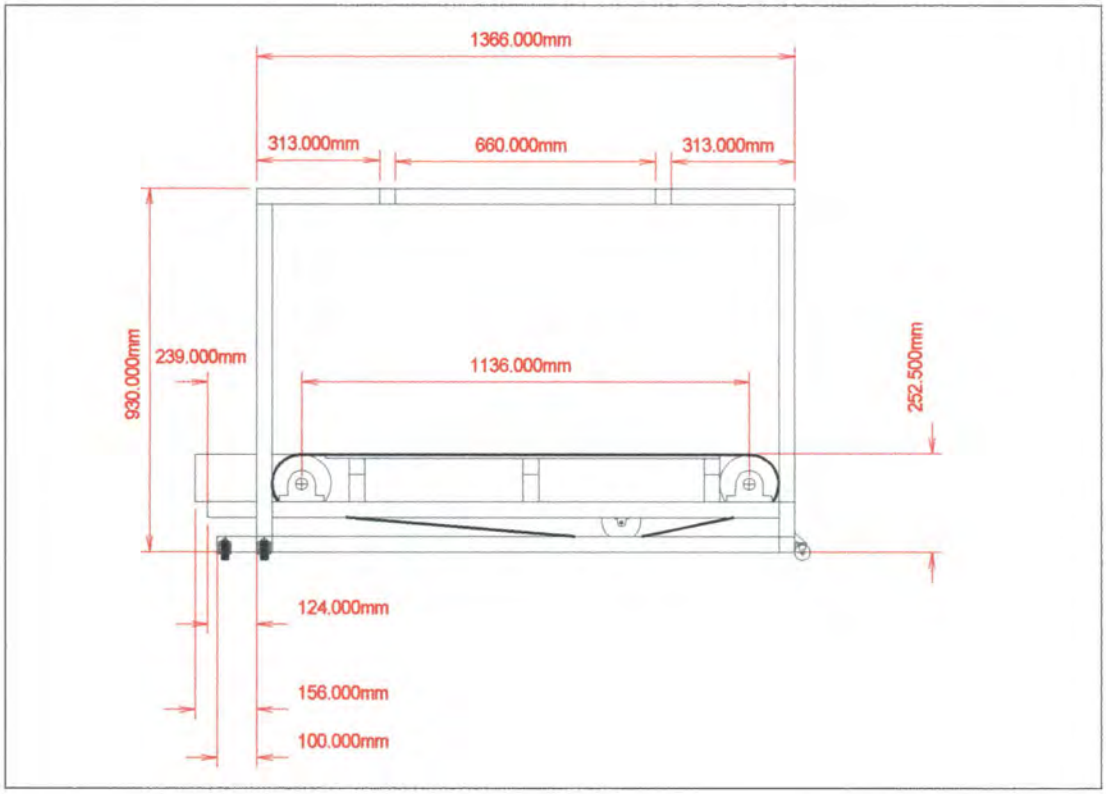
1366.000mm
313.000mm
660.000mm
313.000mm
930.000mm
239.000mm
1136.000mm
252.500mm
124.000mm
156.000mm
100.000mm

APPENDIX B

This Appendix contains relevant drawings for the suction box.

- Figure B-1
- Figure B-2
- Figure B-3
- Figure B-4
- Figure B-5

FIGURE B-1

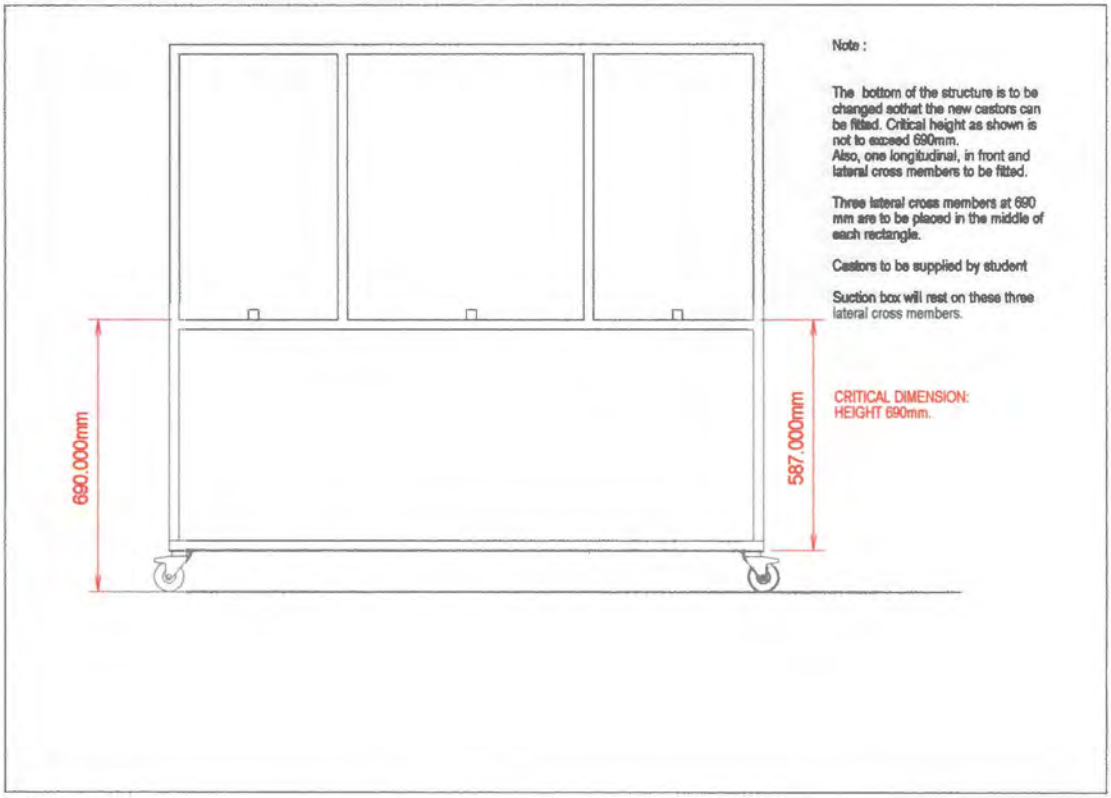
Note :
The bottom of the structure is to be changed sothat the new castors can be fitted. Critical height as shown is not to exceed 690mm.
Also, one longitudinal, in front and lateral cross members to be fitted.
Three lateral cross members at 690 mm are to be placed in the middle of each rectangle.
Castors to be supplied by student
Suction box will rest on these three lateral cross members.
CRITICAL DIMENSION: HEIGHT 690mm.
690.000mm
587.000mm

FIGURE B-2

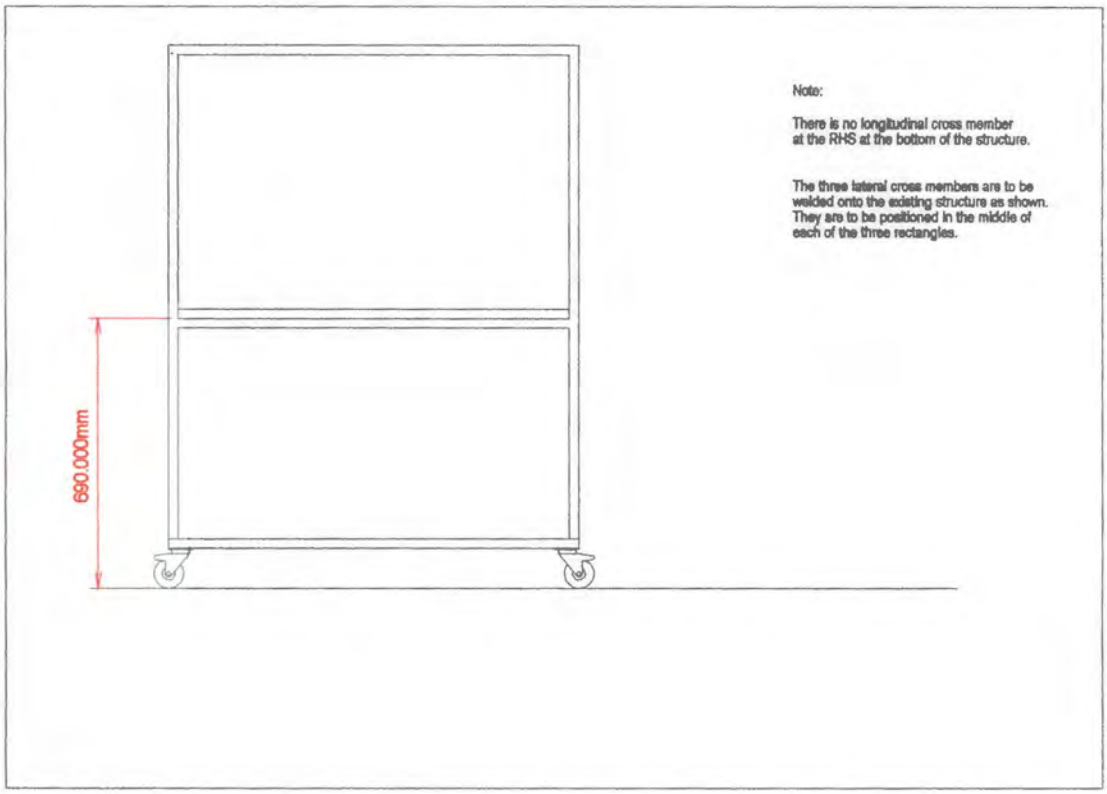
690.000mm
Note:
There is no longitudinal cross member at the RHS at the bottom of the structure.
The three lateral cross members are to be welded onto the existing structure as shown. They are to be positioned in the middle of each of the three rectangles.

FIGURE B-3

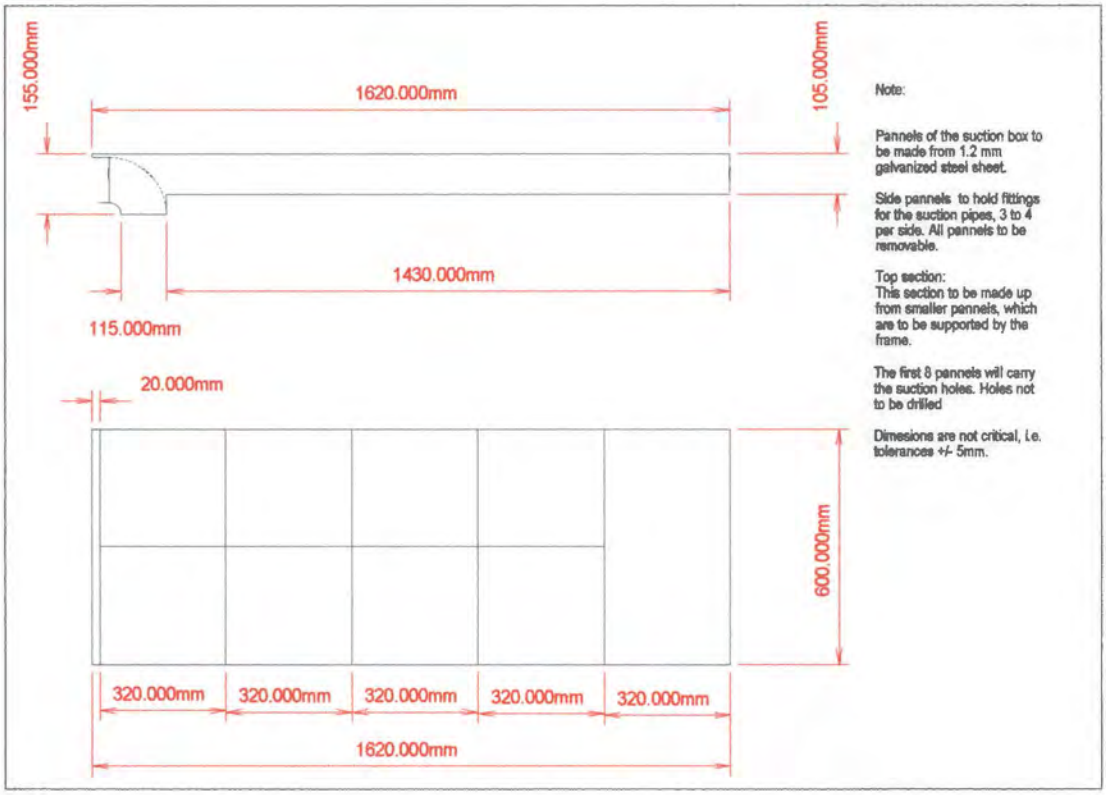
155.000mm
1620.000mm
105.000mm
1430.000mm
115.000mm
20.000mm
600.000mm
320.000mm
320.000mm
320.000mm
320.000mm
320.000mm
1620.000mm
Note:
Pannels of the suction box to be made from 1.2 mm galvanized steel sheet.
Side pannels to hold fittings for the suction pipes, 3 to 4 per side. All pannels to be removable.
Top section:
This section to be made up from smaller pannels, which are to be supported by the frame.
The first 8 pannels will carry the suction holes. Holes not to be drilled
Dimesions are not critical, i.e. tolerances +/- 5mm.

FIGURE B-4

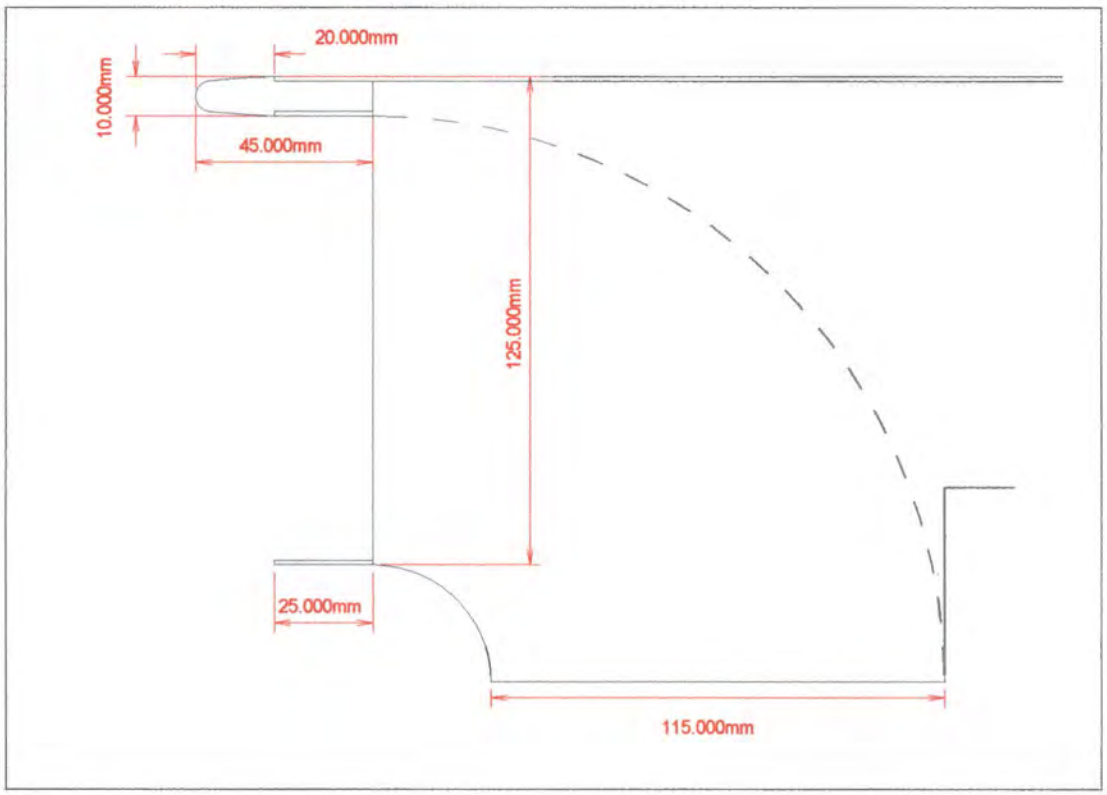

FIGURE B-5

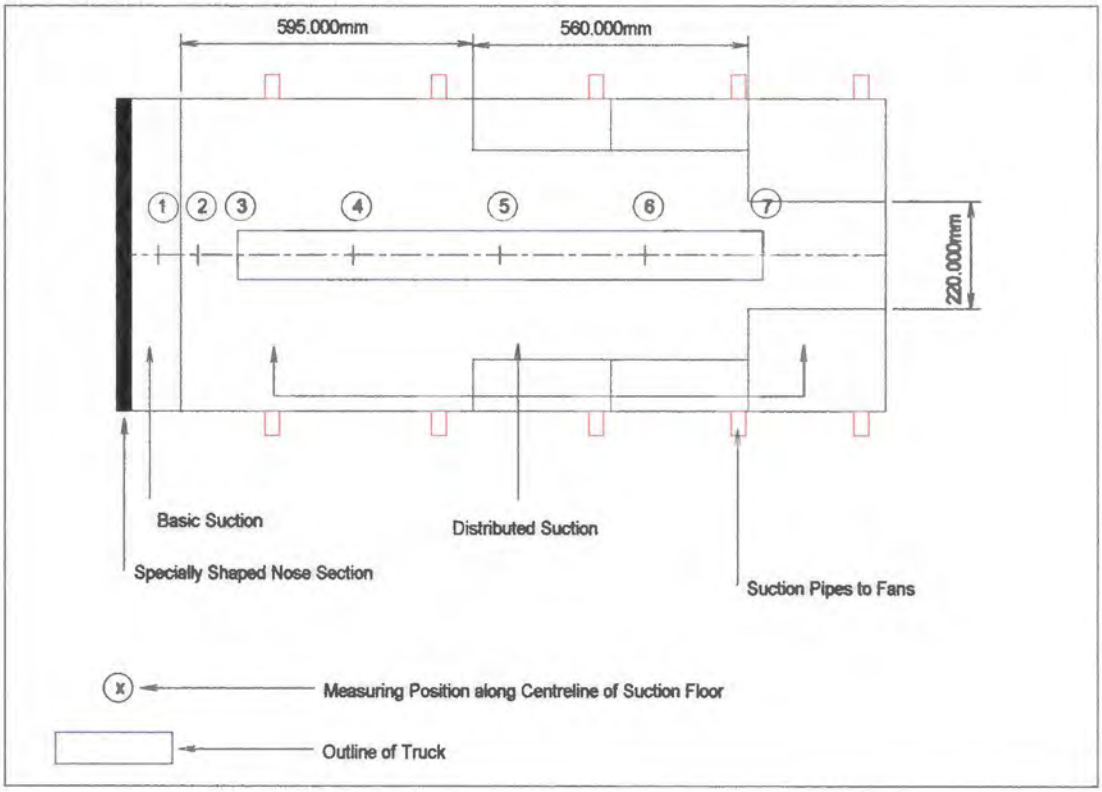
595.000mm
560.000mm
1
2
3
4
5
6
7
220.000mm
Basic Suction
Distributed Suction
Specially Shaped Nose Section
Suction Pipes to Fans
x
Measuring Position along Centreline of Suction Floor
Outline of Truck

APPENDIX C

This appendix contains important photographs taken during the experiments. A short explanation is supplied with each photograph.

FIGURE C-1

Side view of the model in the test section at 8 degrees yaw.

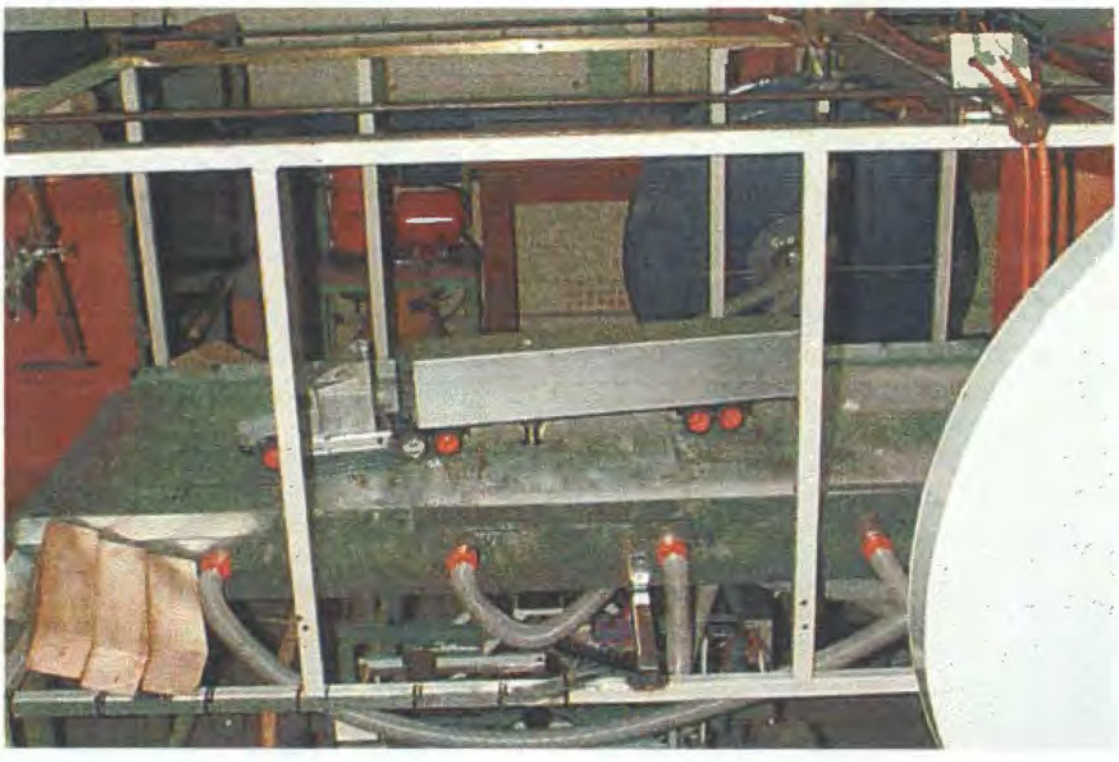

FIGURE C-2

Side view of the horse and front section of the trailer. Also visible on the rhs is the sting.

FIGURE C-3

Open trailer showing the electrical wiring for the motors and locations of sting and motor.

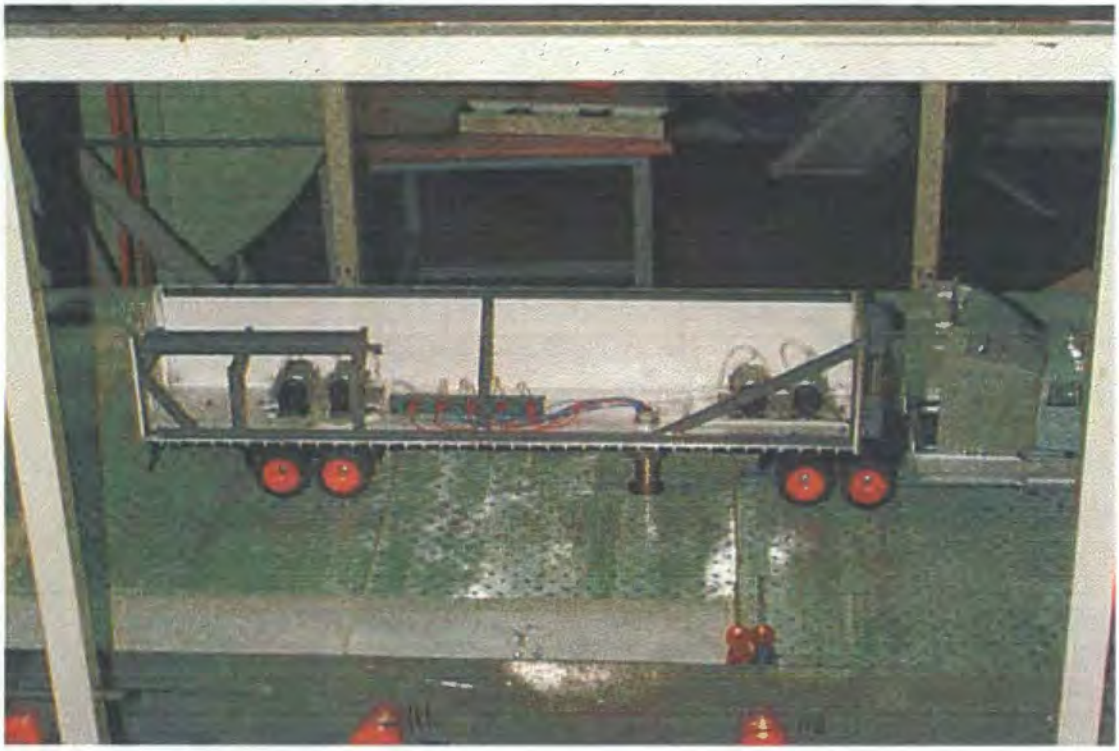

FIGURE C-4

Oblique view of horse with skirts.

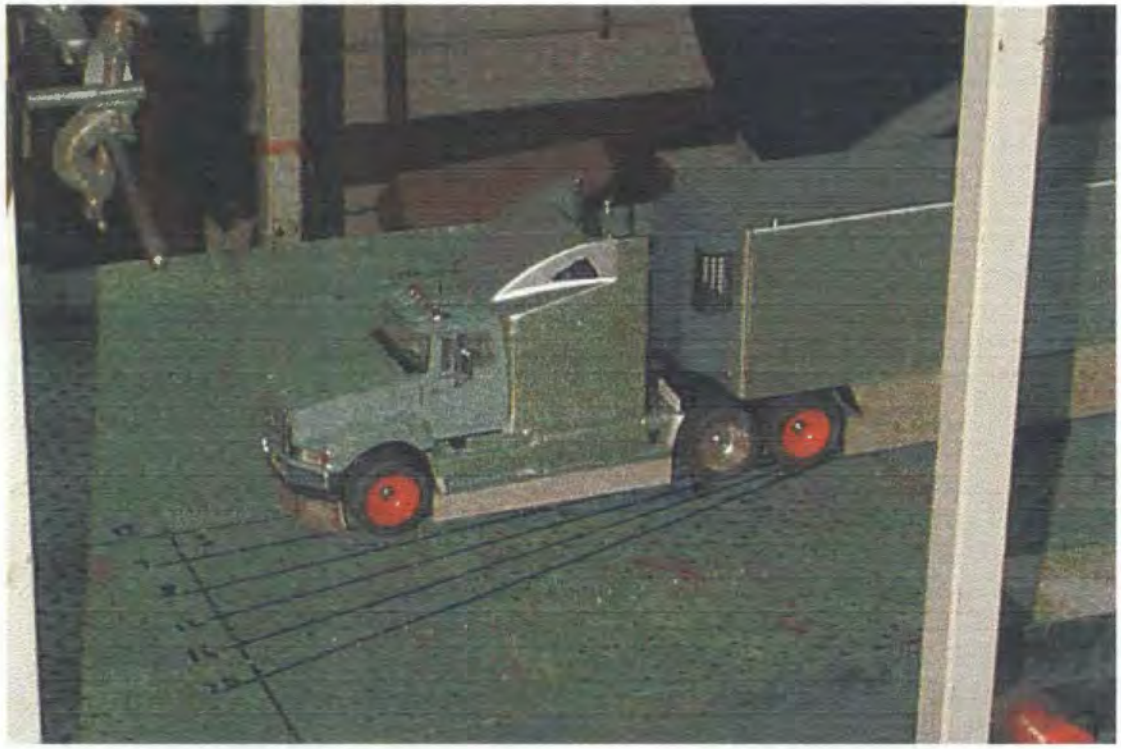

FIGURE C-5

Front view taken from within the wind tunnel showing the horse with skirts and the boundary layer scoop. Also visible are the fences on the side of the suction box.

FIGURE C-6

Front view of the model with skirts at yaw. The boundary layer scoop is visible below the suction surface in the front of the picture.

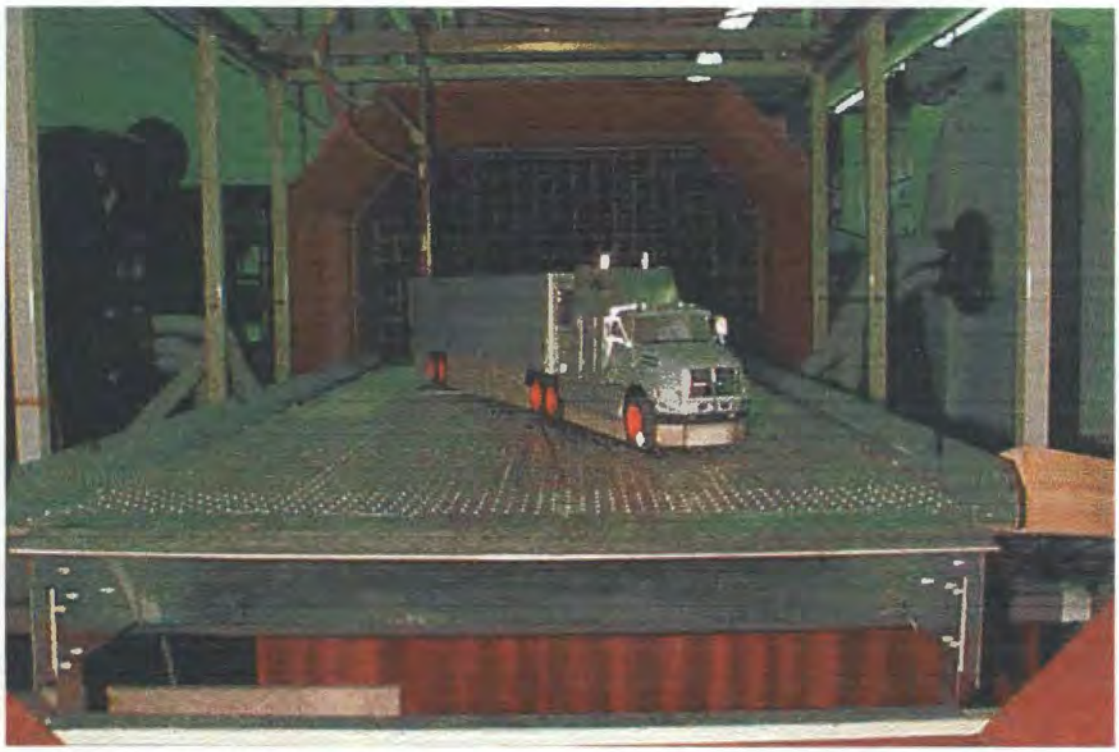

FIGURE C-7

Close up of the model with skirts showing all the details.

FIGURE C-8

This picture is a top view of the assembly. Visible are the patches covering the suction surface were no suction is required.

FIGURE C-9

This shows the traversing sleigh that was used to measure the pressure in the test section.

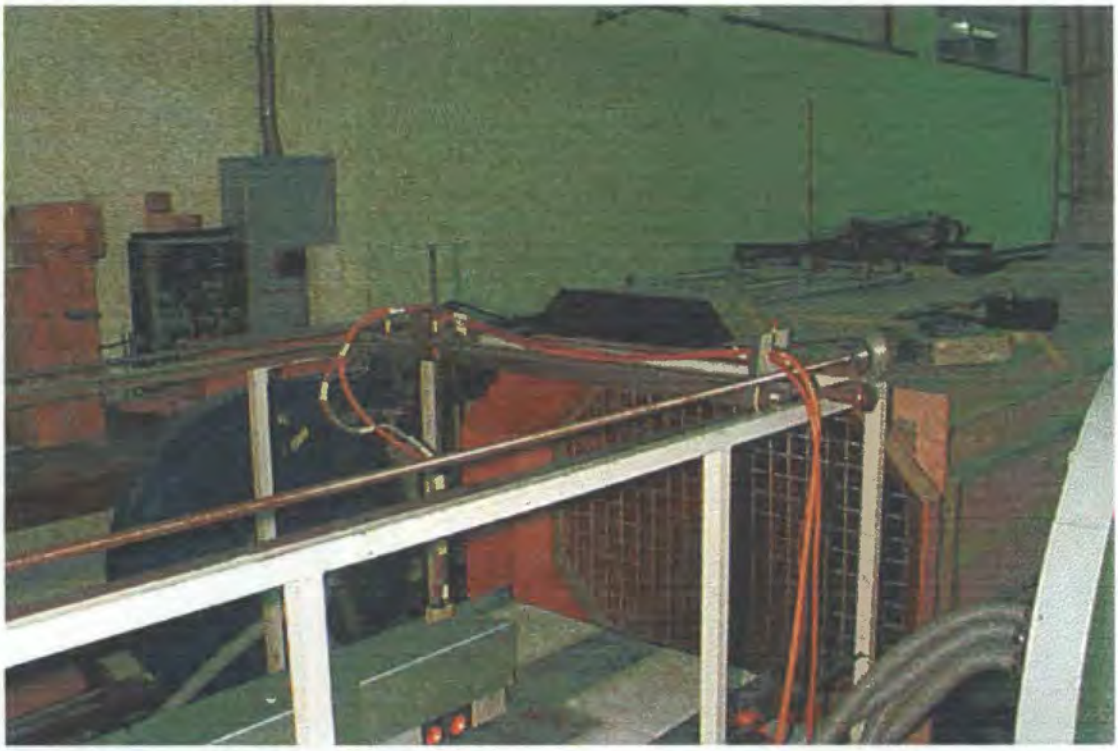

FIGURE C-10

This picture shows the instruments that were used. A digital micromanometer is resting on top of the DC power source. The voltmeter is next to the DC power source. The knob used to control the air speed is below the round pressure gauge on the blue panel.

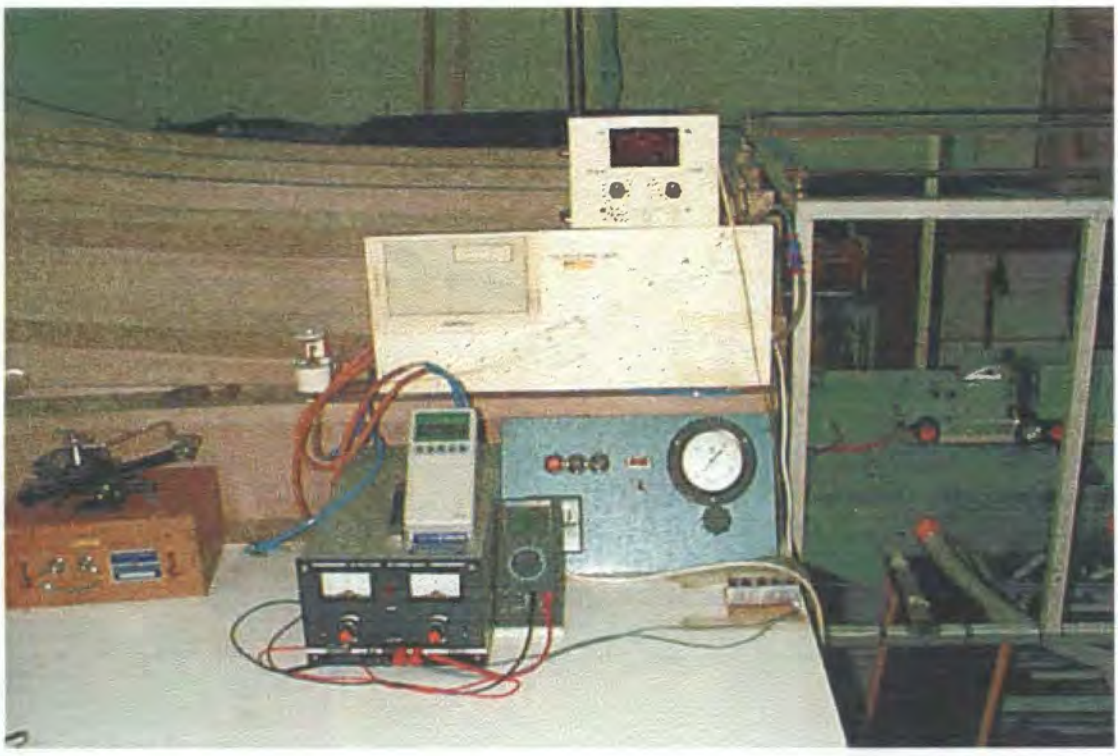

FIGURE C-11

This shows one of the centrifugal fans used to remove the air from the suction box. The manifold required careful selection, because the head losses had to be kept to a minimum to maximise the available suction. Also visible are the grey vacuum hoses that connect the fan to the side of the suction box.

APPENDIX D

This Appendix contains drawings relating to the aluminium frame and axle assembly for the model.

FIGURE D-1

This drawing shows the aluminium axle support for the model.

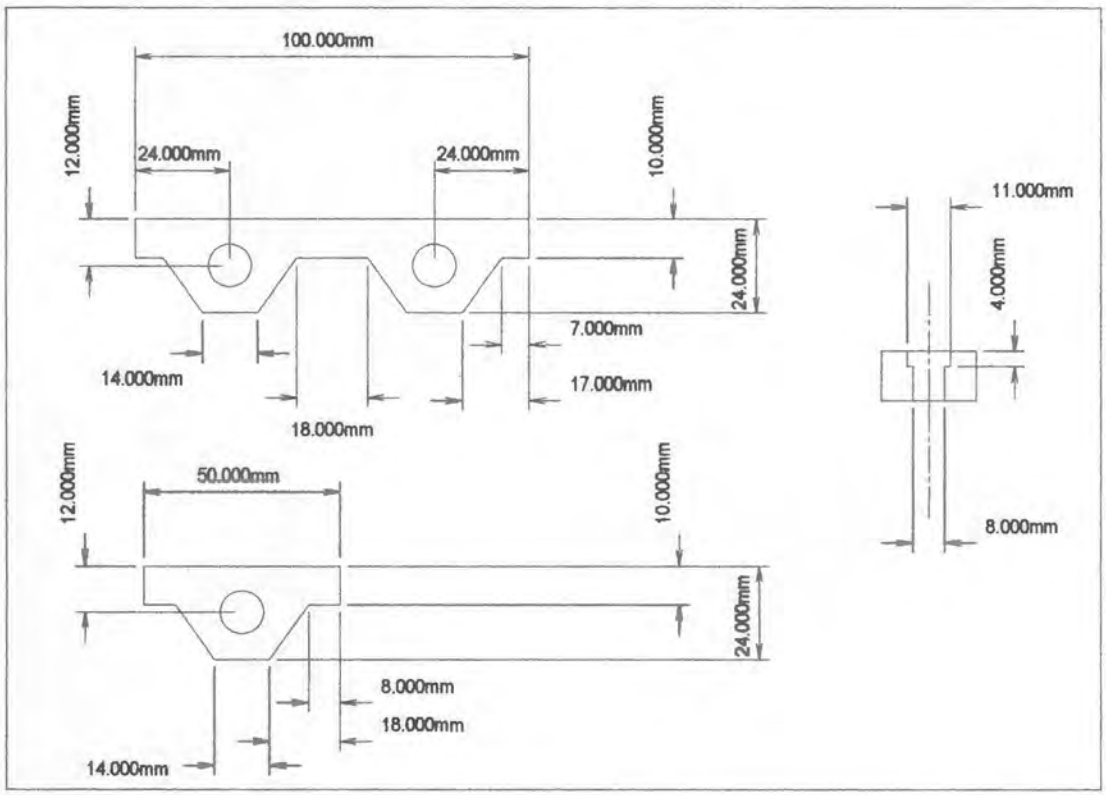

FIGURE D-2

This drawing shows a front view of the aluminium assembly for the model. The bearings holding the steel axles in place and the tyres are indicated.

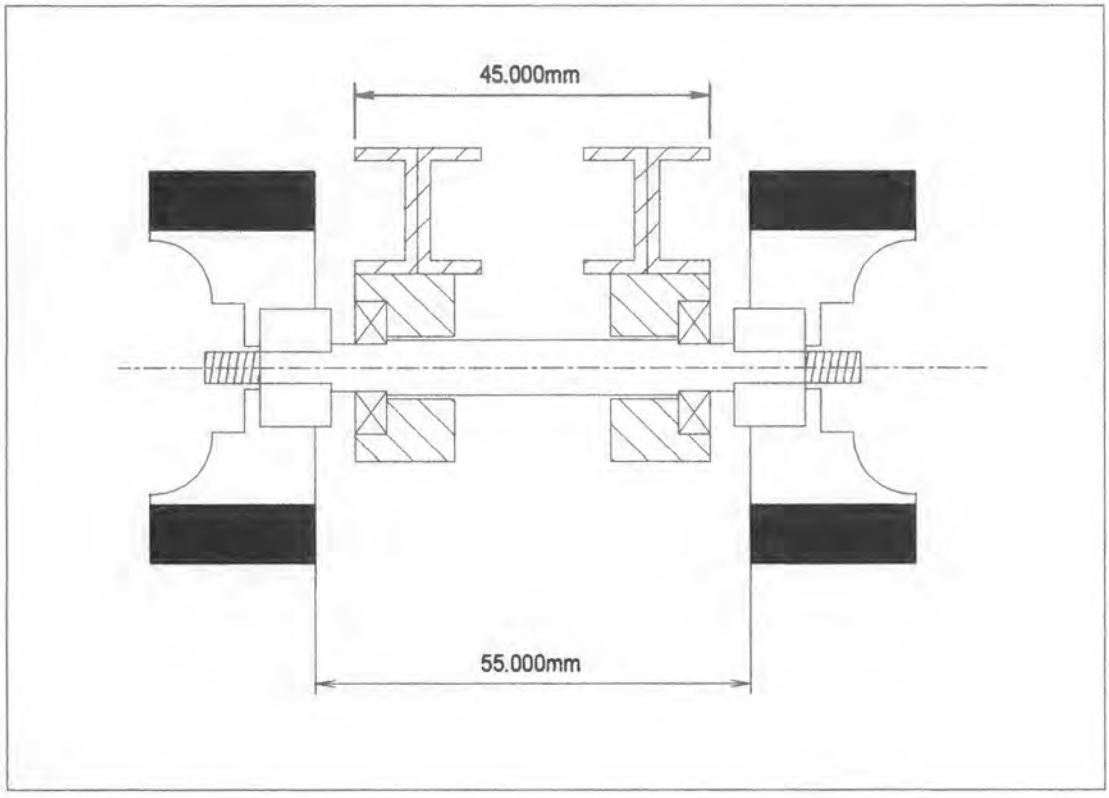

FIGURE D-3

Axle detail.

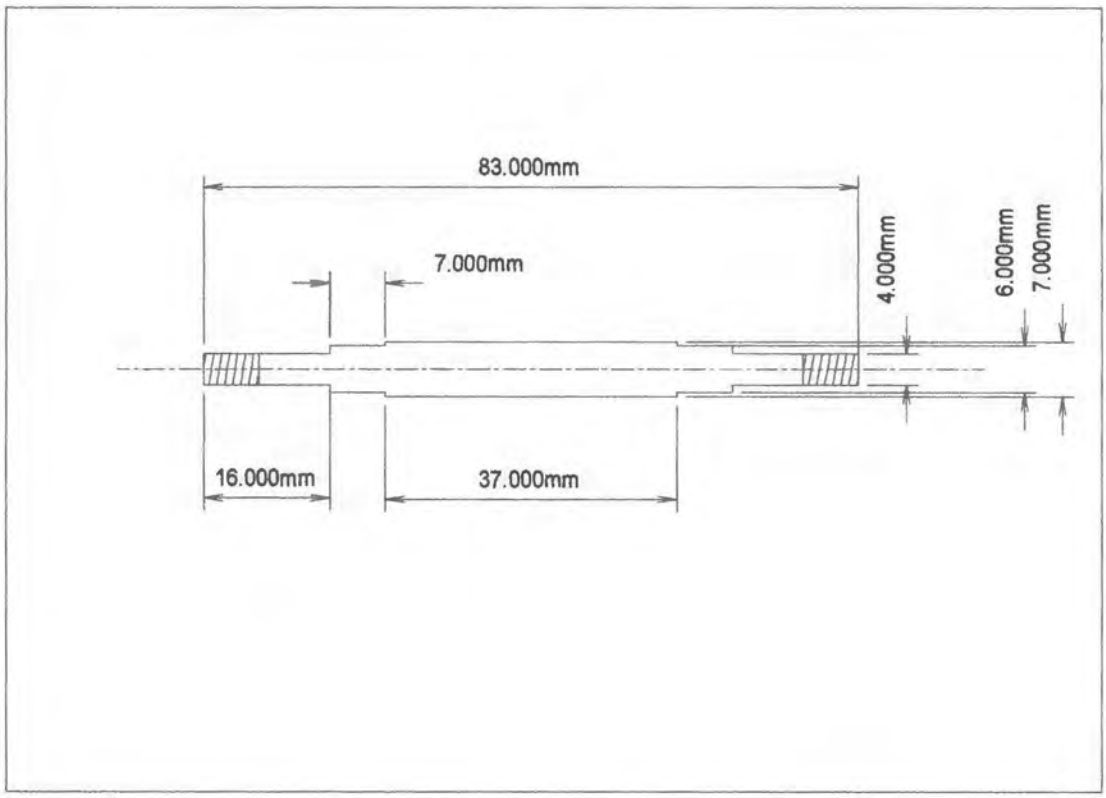

FIGURE D-4

This is a drawing of the larger manifold fitted to the fans. For clarity, the connecting pipes are not shown. It was found that the best flowrate was achieved when the flow was not required to change direction, as would be the case in a 90 degree turn.